STRESS AND STRAIN ANALYSIS FOR DETERMINING THE DEFORMATIONAL HISTORY OF EXPOSED OUTCROPS ALONG BAGNOTAR BARAGALI SECTION, ABBOTABAD, PAKISTAN

By

Maryum Zakir

02112111025

DEPARTMENT OF EARTH SCIENCES
QUAID-I-AZAM UNIVERSITY,
ISLAMABAD.

SESSION: 2021-2023

STRESS AND STRAIN ANALYSIS FOR DETERMININGTHE DEFORMATIONAL HISTORY OF EXPOSED OUTCROPS ALONG BAGNOTAR BARAGALI SECTION, ABBOTABAD, PAKISTAN

A thesis submitted to Quaid-i-Azam University Islamabad in partial fulfillment of requirement for the degree of Master of Philosophy in Geology.

By

Maryum Zakir

Supervised by

Dr. Abbas Ali Naseem

DEPARTMENT OF EARTH SCIENCES
QUAID-I-AZAM UNIVERSITY,
ISLAMABAD.

SESSION: 2021-2023

DEDICATION

In this thesis, I pay tribute to the individuals who have significantly influenced my academic journey and helped shape my perspective towards learning. First and foremost, I dedicate this work to my grandfather Capt.Masood-ur-Rehman(late), my parents, who instilled in me the importance of acquiring knowledge for its intrinsic value and taught me the power of perseverance in overcoming even the most formidable challenges by taking them one step at a time.

Furthermore, I extend my heartfelt gratitude to my project supervisor, who provided unwavering support and guidance throughout my research process. I will always be appreciative of his dedication and commitment towards my growth as a scholar. This dissertation is a testament to his mentorship and the impact he has had on my academiccareer.

ACKNOWLEDGEMENT

With heartfelt gratitude and a deep sense of faith, I express my appreciation to the Creator, Allah Almighty, who has blessed me with the ability to undertake and successfully complete my research work. I extend my reverence to the Holy Prophet Muhammad (PBUH), who illuminated the path to knowledge and understanding of our Creator.

I would like to express my profound gratitude to my supervisor, **Dr Abbas Ali Naseem**, for his unwavering support and guidance throughout my research journey. His encouragement and motivation were crucial to my progress, particularly during times when the road ahead seemed challenging. I am deeply thankful for his contributions, as the present research work would not have been possible without his expert supervision, guidance, and constant encouragement.

I would like to extend my gratitude to the individuals who have played a pivotal role in the successful completion of my research and this thesis. My mother's unwavering support and encouragement was invaluable and greatly contributed to my progress. I am also thankful to my teachers who provided guidance and insights that helped shape my understanding of the subject matter. Additionally, I am grateful to my family members for their support and understanding during this journey.

I would also like to express my appreciation to the Department of Earth Sciences for providing me with the opportunity to conduct this work and further my education in this field. Finally, I would like to thank my friends especially Asif Ullah, Zubair Ahmed and Qurat-ul-Ain for their assistance and support during my research. Their contributions have been greatly appreciated and instrumental in helping me reach this milestone.

(Maryum Zakir)

Table of Contents

LIST OF FIGURES

LIST OF TABLES

Abstract

The current study focuses on the deformational history concluded form the interplay of strain and stress associated within the folded strata exposed along the Bagnotar-Baragali Section, north Pakistan. A field-based approach is combined with the lab analysis for interpreting the relation of stress and strain. Detailed fieldwork is conducted and collectively twenty different oriented samples are collected from the folded units exposed in the study area. Strains markers i.e., Ooids are studied from shape and orientation for deducing the strain ellipsoid or ellipse through computer generated model by Ellipse fit application. The finite strain of rocks having fabric that indicates history of deformation associated with the rocks. Stress is calculated from field dataset also interpreted and correlated with the deformational history. The Rf/ϕ plot method is used for the ellipticity measure. The strain ratio R and orientation f of the heavily deformed elliptical ooids are summarized and interpreted. The variations are fewer than 90 degrees. The region's strain ratios and angular strains are defined by a mean orientation 25.6^0 regarding true north and maximum shortening observed is 19.50% calculated from oriented samples having ooids as strainmarkers . The results further show that, the direction of deformed elliptic ooids observed in the SamanaSuk Formation represents the region's stacked tectonic processes. The Rf/Phi model plot is helpful in determining the modification of bedding horizontally and vertically damaged elliptical ooids. Microscopic to mesoscopic structural shortening are parallel to the local tectonic fabric. The intermediate stresses acting on the formation are NE-SW directed. The NEE-SWW directed stresses are minor stresses acting on the formation. While majority of the fractures are oriented in NW-SE direction, while minimal number of fractures are oriented in NE-SW direction. Folding which is observed in the SamanaSuk Formation of Jurassic age which is exposed along bagnotar baragali section as the magnitude of stresses increases deformation exceeds maximum ductility limit and fractures are produced.

Chapter .1 Introduction

1.1 General description

The present study focuses on analyzing the microscopic strains along the Bagnotar Thrust in the Bagnotar area of Abbottabad. The study region is situated within the Abbottabad district in the Khyber Pakhtunkhwa province of Pakistan(Shahzada, Naseer, and Javed 2012) (Raza et al. 2011). Tectonically, it is positioned within an arc-shaped mountain range that extends from Afghanistan in the west to Nepal in the east (MonaLisa, (Nov, 2005)) (Hameed, Khan, and Dentith 2023) (M. P. Searle, 2012) The Indian-Eurasiancollision has led to the deformation of thick Phanerozoic sequences along with the formation of igneous intrusions and metamorphic processes (Drona Adhikari, 2021)(Searle, Robb, and Gardiner 2016) (Ali et al. 2021)

Abbottabad lies within the Abbottabad block, which is part of the southern Himalayan fold and thrust belt located in the northwestern Himalayas of Pakistan(Ghazi et al. 2015) (AKHTAR et al. 2019) (Muhammad Qasim, 2014) This region is bordered to the north by the Main Central Thrust, to the southeast by the Main Boundary Thrust, and to the west by the Indus River. In terms of stratigraphy, the rocks in the study area range in age from Precambrian to Eocene (Saboor, 2020)(Ali et al. 2021) (Kazmi, 1997) (MonaLisa, (Nov, 2005))

Several studies have been conducted in the Bagnotar area, including investigations into the sedimentological attributes of the area and the SamanaSuk Formation from the Middle Jurassic period (Saboor, 2020). Other studies have explored the impact of dolomitization on the reservoir heterogeneities of the SamanaSuk Formation in the NW Himalaya (Mumtaz, 2018) and the microfacies and diagenetic fabrics of the formation at the Harnoi section in Abbottabad, Khyber Pakhtunkhwa (Shahid Hussain, 2018).

The area has undergone several tectonic events, leading to different stages of deformation such as folding, faulting, and fracturing(AKHTAR et al. 2019; Ali et al. 2021; Qasim, Khan, and Haneef 2014) (Jan, 2020)(Bossart et al. 1988) as shown in figure 1-1(Available from: https://www.researchgate.net/figure/Tectonic-Map-of-Northern-Pakistan-Showing-Major-Structural-boundaries-and-study-area_fig1_274707540 [accessed 11 Apr, 2023]) which can be observed at all scales from regional to microscopic in the rocks along the fold belt. Nathiagali and Bagnotar Thrust are the major thrusts in this area (Shamim et al., 2019), but microscopic

analysis has received less attention. The current study, therefore, focuses on the analysis of strain and stress along the exposed formations, where the Hazara Formation is thrust over the SamanaSuk Formation in the Dhamtur syncline that exists in the fold and thrust belt. The progressive shortening and repetition of strata is evidence of folding in the area.

The Bagnotar Thrust is roughly east-west oriented, consisting of several undulations and bends with a dip of 50 to 60 degrees. The study aims to determine the direction and magnitude of finite strain, which will then be used to interpret the kinematic history and tectonic processes of deformation stored in the rocks in the area.

Available from: https://www.researchgate.net/figure/Tectonic-Map-of-Northern-Pakistan-Showing-Major-Structural-boundaries-and-study-area_fig1_274707540 [accessed 11 Apr, 2023])

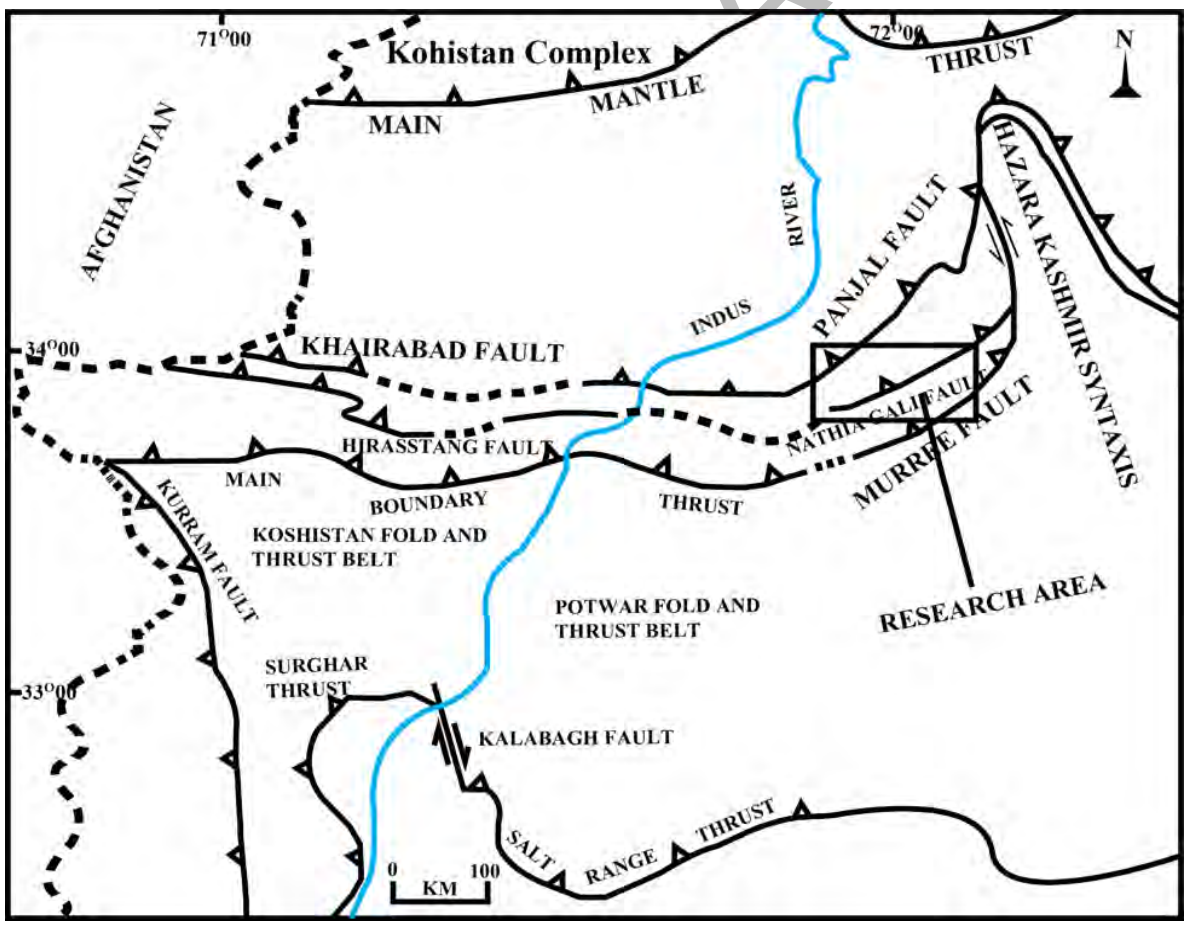

Figure 1-1: showing the geological map of Northern Pakistan including the Research area. (Hussain, (2013))

1.2 Methodology

The field studies performed aimed to investigate the stages of deformation resulting from tectonic folding and faulting. A systematic sampling was carried out along a 3.5 km transect with 20-meter intervals, leading to the collection of 20 samples. The samples were processed in the rock cutting laboratory of the Department of Earth Sciences at Quaid e Azam University Islamabad to prepare thin sections. The thin sections were analyzed using microscopic techniques to identify strain markers, such as ooids and fossils, and to calculate finite strain using Rf/φ methods (Ahmad, oct 2017) (De Paor 1980). Fractures were analyzed to determine the stress state of the rocks by collecting surface fracture data, including direction, dip/strike, fracture density, frequency, and distribution. The information was obtained from 198 distinct sites, each with 75 fracture inventory measurements, and was used to calculate the total stress regime and deformation. The results of the study will be used to make predictions about future deformation.

1.3 Location and accessibility

The Bagnotar area is located 11.5 kilometers southeast of the city of Abbottabad, in the province of Khyber-Pakhtunkhwa, with coordinates 34°10' 7.5036° N and 73°13' 17.3892° E (Anon (March 28)). The area has a total area of 18,013 square kilometers and is approximately 61 kilometers northeast of Rawalpindi. Abbottabad lies at a plateau near the south corner of the Rash plain and offers a route to the Kaghan Valley (contributors., (2023).). The region is connected to the Indus plain and Kashmir region via road and rail networks, with a rail connection to Peshawar at Havelian ,N-35 and S-2 connecting from different cities nearby as shown in figure 1-2.The natural beauty of Abbottabad, with its stunning views and proximity to the Karakorum and Himalayan ranges, is unmatched. The topography of the area consists of both mountainous ranges and plains, with mountains running from north to south to the north of Abbottabad, situated south of the Kabul River, which intersects the province from east to west. (Britannica, 2015)

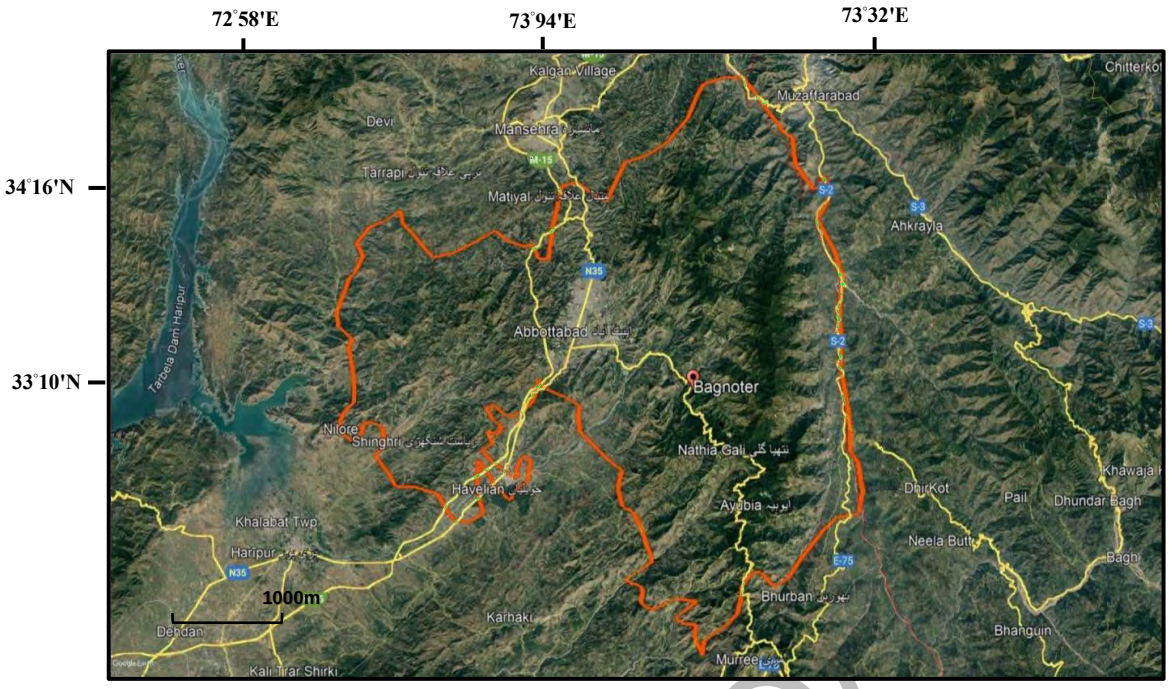

Figure 1-2: Showing Location and accessibility map of Abbottabad (Google earth generated) showing nearby areas and N-35 and S-2 connecting from different cities nearby

1.4 Aims and objectives

The current study aims to examine the stages of deformation by analyzing the strain from strain markers like ooids and the stress from fractures in the exposed SamanaSuk and Kawagarh Formations in the Bagnotar-Baragali area. The goal is to understand the correlation between the regional stress direction and the microscopic strain and stress stored in the rocks. This information can provide insights into the tectonic changes that have affected the morphology of the major thrust faults and the fold-thrust belt, which is currently understudied. By analyzing the deformational facts at all levels, it may be possible to estimate the future deformational regime of the faults in this region.

Chapter .2 Regional Tectonics

2.1 Tectonics zones of Pakistan

The deformation of the Earth's crust over a wide region is referred to as regional tectonics. In Pakistan, the collision of the Indian and Eurasian plates is the main force behind the regional tectonic movements. This collision has caused the uplift of the Himalayan Mountain range and the formation of other tectonic features. (Kazmi, 1997) (Jan, 2020) (MonaLisa, (Nov, 2005))

Pakistan can be divided into several tectonic zones based on its features resulting in tectonics, structural geology, history of tectonic activities, and lithofacies(Ghazi et al. 2015) (Kazmi, 1997) (M. P. Searle, 2012). These zones are the Indus Platform and foredeep, the Northern-western folding and thrust belt of Himalaya, the Koshistan magmatic Tibetan range, the flysh basin of khorasaan and Accretionary Zone of Makran, the Chaghai, and the Pakistan shoreside.(Ali et al. 2015, 2021; Bossart et al. 1988)

The Indus Foredeep is a vast and relatively flat area located in northern Pakistan. This region is characterized by sedimentary rocks that were laid down in a shallow ocean during the Paleocene and Eocene periods (Edward A. Johnson, 1999). Additionally, the foredeep is a section of this area where deeper sedimentary rocks can be found, which were formed as a result of the impact of the Indo-Asian lithospheric plates(Khan and Liu 2019)

The Northwest Himalayan fold-and-thrust belt is a region in northern Pakistan featuring mountain ranges and valleys (Kazmi, 1997)(Ali et al. 2021). It is distinguished by the folding and thrusting of the Earth's crust, as well as volcanic activity and changes in the minerals and textures of rocks due to high pressures and temperatures. (Drona Adhikari, 2021) (M. P. Searle, 2012)

The Koshistan-Ladakh magmatic arc is a region in northern Pakistan comprised of mountain ranges. It is marked by the formation of new rock through the solidification of molten material. (MonaLisa, (Nov, 2005)) (M. P. Searle, 2012)

The Karakoram block is a region of mountain ranges in northern Pakistan that has a complex tectonic history, including multiple episodes of folding and thrusting of the Earth's crust (M. P. Searle, 2012).

The Kakar Khorasaan flysh basin and Makran Accretionary Zone are regions located in southern Pakistan. The flysh basin is a region of sedimentary rocks formed by the accumulation of sediments in a shallow sea(Hussain et al. 2013; Samira et al. 2019). The Makran Accretionary zone is a region of deformed rocks that resulted from the collision of tectonic plates. (M. Sadiq Malkani, 2017)

The Chaghai magmatic arc is a region of mountain ranges in western Pakistan marked by the

Formation of new rock through the solidification of molten material (Edward A. Johnson, 1999) (M. Sadiq Malkani, 2017) (Kazmi, 1997)

The Pakistan offshore is a region located in the Arabian Sea off the coast of Pakistan and is defined by sedimentary rocks that were deposited in a shallow sea(Khan et al. 2016) (Kazmi, 1997)(Baig et al. 2022)

The fold-and-thrust belt of Northwestern Himalaya spans an area of approximately 250 km wide and 560 km long. It is a long chain of mountain ranges that starts from the Afghan border near Parachinar and extends all the way to the Kashmir Basin. The eastern boundary of this region is formed by Nanga Parbat and Hazara-Kashmir Syntaxes.(Ali et al. 2015, 2021; Hameed et al. 2023) The fold-and-thrust belt encompasses the entire region between the Main Mantle and the Upper Mantle, with the Main Mantle to the north and the Salt Range Thrust to the south. This area encompasses several mountain ranges including Nanga Parbat, Hazara, southern Kohistan, Swat, Kalachitta, Margalla, Kohat, Sufaid Koh, Salt Range, and its western extension. (Kazmi, 1997) (Jan, 2020) (M. P. Searle, 2012)

2.2 Tectonic settings, NW Himalayas of Pakistan

In northern Pakistan Himalayas have four subdivisions (Farah et al., 1984; Yeats and Lawrence, 1984; Ali et al. 2021). Tectonic settings of region have been shown in figure.2-1.

These are from north to south;

1. The Hindukush and Karakoram mountain ranges
2. The Kohistan Island arc is located between both the MKT and MMT (Tabir Kheli, 1982; Farah et al .1984)
3. The Swat, Hazara, and Kashmir low mountains lie in the MMT and MBT (Searle and

Treloar 2019) (P. K. Zeitler, 1994)

4. The Coastal Region and Potwar Plain to the southeast of the MBT reflect the Sub Himalayan eastern flank and thrust zone(Searle and Treloar 2019).

Scientific Figure on ResearchGate. Available from:
https://www.researchgate.net/figure/Regional-tectonic-map-showing-the-major-fault-systems-in-northern-Pakistan-The_fig2_256838591 [accessed 11 Apr, 2023]

Figure 2.1 Regional tectonics of North West Himalayas

2.2.1 Hazara Kashmir Syntaxis (HKS)

The Hazara-Kashmir Syntaxis is a trending anti-form located in the westernHimalayas. It separates the Higher, Lesser, and lower Himalayas, it is a significant curve in the western

Syntaxis of the Himalayan mountain range(AKHTAR et al. 2019; Ali et al. 2015; Bossart et al. 1988) .There are two bends in the western Syntaxis, the northern bend being known as the Nanga Parbat Syntaxis and the southern bend being referred to as the Hazara Kashmir Syntaxis.(Bossart et al. 1988)

Unlike traditional anticlines, the Hazara-Kashmir Syntaxis has its core or center contains younger and its extremeties having older strata, because of the effects of before development thrusting. This makes it youngest of tectonic features in the region, and all major thrusts, including the MBT, MCT, and Panjal Thrust, are refolded by it.(Bossart et al. 1988; Calkins 1967)

(a) Structural options

The Hazara-Kashmir Syntaxis region is highly dynamic due to its tectonic activity and its location within the mountain range. The area is dominated by strong tectonic forces and as a result, it exhibits a wide range of structural features that range from microscopic to macroscopic in scale(Ali et al. 2015; Calkins 1967). Some of the most notable structural features of this region are discussed below.

(b) Muzaffarabad anticline

The Northern region of the Hazara-Kashmir Syntaxis is characterized by a significant doubly plunging anticline with well-defined limbs, located to the north of the Jehlum River(Ali et al. 2015) (Ahmad, oct 2017). This feature is highly impacted by tectonic forces and is considered an important aspect of the area.

(c) Muzaffarabad thrust (Jehlum thrust)

The Muzaffarabad Thrust is a highly inclined surface that is visible to the east of Muzaffarabad. It ranges from a slope of 25 to 50 degrees and extends to the Balakot region, where it meets with the Thrust fault of Panjal and MBT at the western boundary of the Syntaxis (Jan, 2020) (MonaLisa, (Nov, 2005)). It has been re-folded along the Nelam Stream and forms the margins of the Hazara-Kashmir Syntaxis. (Jan, 2020)

2.2.2 Main boundary thrust (MBT)

The MBT outlines the northern margins of the Hazara-Kashmir Syntaxis, located north of Balakot. Near Paras in Kaghan depression, a tectonic slice around two kilometers thick can be found, consisting of carbonates from the Jurassic to Eocene epoch that contact with the Murree Formation within the Hazara Kashmir Syntaxis core (Kazmi, 1997) (M. P. Searle, 2012). This setup fits the definition of MBT as a thrust contact between the Mesozoic-Eocene carbonate platform and the Miocene Molasse sediments of the Murree Formation(Samira et al. 2019).

(a) Western limb

The western margins of the Hazara-Kashmir Syntaxis are more complex than the eastern margin(Ali et al. 2015). The MBT and Panjal thrust merge near Balakot and continue southward as one fault, while remaining separate entities on the eastern margins and at the northern apex of the Syntaxis.(Calkins 1967)

(b) Jehlum Fault

The Jhelum Fault is a north-south homeward-bound steep/upright left lateral fault which indicates southward extremity of the west arm of the Syntaxis(Calkins 1967). It can be found south of Muzaffarabad and roughly lines the Jehlum stream from Muzaffarabad to Kohala.(Ali et al. 2015)

2.3 Stratigraphy

Stratigraphy of harnoi nathiagali section have been discussed here with oldest rock exposed area is Precambrian the Hazara Formation(Qasim et al. 2014) after that Triassic and Permian sequence is missing (Umar, 2014), exposed unit is the Samanasuk Formation of Jurassic(Hussain et al. 2013) and Chichali Formation, Lumshival and Kawagarh Formation of Cretaceous is also exposed(Shah 1977) shown in figure 2-1.

2.3.1 Pre-Cambrian succession

(a) Tanawal Formation

The Tanawal Formation (Wynne,1879) used term “Tanawal Group” is a sequence of rocks located in the area north and east of the Tanawal Formation is primarily composed of quartzose schist, quartzite, and in some areas, there are layers and lenses of quartzose

conglomerate(Wynne,A.B. 1879). The rock unit mostly comprised of moderately sized grains of quartzite and thinly layered finely grained of schist with a low to medium level of metamorphism(Qasim et al. 2014; Shah 1977).

(b) Hazara Formation

The formation known as "Slate series" was first named by Mark and All in 1961. This formation was referred to as "Hazara slate" by Middlemiss in 1896 and later as "Hamra Formation" by Calkins et al. in 1969. Latif (1970) named it "Hamra Group". The Hazara formation is composed of phyllites, slate, and shale, with occasional graphite layers and limestone. (M. Sadiq Malkani, 2017) (Umar, 2014)The green to dark green and black phyllite and shale exhibit rusty brown and dark green colors when weathered.(AKHTAR et al. 2019)

(c) Samanasuk Formation

The Jurassic series includes the Samana Suk Formation that is made up of limestone that has an unconformable contact with the Hazara Slates. Makes up the unit is mostly made up of limestone and marls and some sandstone intervals it is marked as the significant unit of upper indus basin(Hussain et al. 2013)

2.3.2 Cretaceous succession

Comprised of thin to thick-bedded dolomite, limestone, and iron rich igneous, sandy, and oolitic beds.(Fatmi, A. N., 1971) It has a thickness about190m to 366m in the Bagnotar section in the Hazara area and the Chichali Formation is not comformable. (M. Sadiq Malkani, 2017)

(a) Chichali Formation

It encompasses rocks that sit on top of the SamanaSuk Formation. It consists of a mixture of silty shale, sandstone, and shale, with a range of variations in composition and thickness. The lower part of the formation includes glauconitic sandstone and a nodular silty, calcareous, and phosphatic base, while the upper part is comprised of dark pyritic shale without fossils.(Anjum et al. 2022) (AKHTAR et al. 2019)The thickness of the formation varies, with a thickness of 33m in southern Hazara and increasing to 64m in the northwest of Kalapani. (Hussain, (2013)) (M. Sadiq Malkani, 2017)

(b) Lumshiwal formation

The Lumshiwal Formation is a geological formation that was initially named the "Giumal Sandstone" by Middlemiss in 1896. However, it was later renamed as the "Lumshiwal Formation" by Cotter in 1933. The Lumshiwal Formation is characterized by variations in its lithology and thickness, which have been studied at the Jhamiri Village section. (M. Sadiq Malkani, 2017)

The type section of the Lumshiwal Formation is located in Lumshiwal Nala and has been the focus of extensive research and study due to its unique composition and variations in thickness.(Shah 1977) The formation is of great interest to geologists and geomorphologists, and continues to be the subject of ongoing research and analysis.

(c) Kawagarh Formation

The Kawagarh Formation is a geological formation recognized by the Stratigraphic Committee of Pakistan. It was first identified by the Attack Oil Company in a report on Kawagarh Hill in the northern Kala Chitta Range, and originally referred to as the "Kawagarh Marls".

Overall, the Kawagarh Formation is of great interest to geologists and geomorphologists, as it provides valuable information about the geological history and formation of the region. Further research and analysis of the formation will continue to shed light on its significance and importance.

2.3.3 Paleocene succession

(a) Hangu Formation

The Hangu Formation is visible both on the surface and in the subsurface of the Hazara region, and is approximately 35 meters thick at Mandcha Banni in Hazara. The formation has been dated to the Early Paleocene period based on the presence of various fossils, including foraminifers, algae, corals, mollusks, and echinoids.

The Hangu Formation is of significant scientific interest and continues to be the subject of ongoing research and analysis. Its unique composition, presence in the Hazara region, and connection to the Paleocene period provide valuable information to geologists and geomorphologists about the geological history and formation of the region.

(b) Lockhart Formation.

The Lockhart Formation is composed of black and dark grey colored limestone with interspersed marls and shale. It is often bituminous and gives off a foul odor when freshly exposed. The thickness of the formation varies from 90 to 242 meters, according to a study by Shah in 2009.

The Lockhart Limestone lies above the Hangu Formation and below the Patala Formation. (M. Sadiq Malkani, 2017) The age of the Formation has been determined to be Early to Middle Paleocene based on the presence of various fossils, including foraminifers, algae, corals, mollusks, and echinoids.(Khan and , Osman Salad Hersi and Sajjad Ahmed 2017)

The Lockhart Limestone is an important geological formation that provides valuable insights into the geological history and evolution of the region. Its unique composition and relationship to other geological formations have made it a subject of ongoing research and analysis by geologists and geomorphologists.

(c) Patala Formation

Patala formation recognized in Pakistan. The formation is characterized by greenish coloured shale having interbeds of limestone which is nodular. According to Shah (2009), the thickness of the formation ranges from 60 to 182 meters. Latif (1970), Including species such as Globoratalia elongate, Glohigerina Primitive, Triloculinatrigonula, Rotalia, Trochidofonnis, and Miscellanea Prehaimei.(Tariq Shakoor, n.d.)

2.3.4 Eocene Succession

(a) Margalla Hill Limestone

The committee of stratigraphy officially recognized the name "Margalla Hill Limestone" Formation consists of various foraminifers such as Discocyclinaranikitenses, Alveolina, Assilina granulosa, Assilina spinosa, Assilina laminose, Assilinasubspinosa, Tanikothaliasindensis, and Nummulitesmamillatus (Edward A. Johnson, 1999). Its lower and upper contacts are conformable with the Patala Formation and Chorgali Formation, respectively (M. Sadiq Malkani, 2017).

Table 2-1: Showing stratigraphic column of Harnoi-Nathiagali section

	Age	Formation	Description
Cenozoic	Late Paleocen	Patala	Limestone and Shale
	Middle Paleocen	Lockhart	Nodular limestone with shales and marls
	Early Paleocen	Hangu	Sandstone
Mesozoic	Late Cretaceous	Kawagrh	Limestone with marls intervals
	Early to middle Cretaceous	Lamschiwal	Siltstone Sandstone with shale layers
	Late jurassic to early Cretaceous	Chichali	Glauconitic shale and sandstone
	Middle jurassic	Samanasuk	Limestone with Dolomite Patches
	Pre Cambrian	Hazara	Slates phyllite and shale with minor graphite

.

Chapter .3 Methodology

3.1 General Outline

A detailed field based, and desk study approach was adopted for this research. During field work a total of 20 samples have been collected from best exposed Samanasuk formation (Js) and subsequently thin sections were prepared in rock cutting laboratory of Department of Earth sciences Quaid e Azam University Islamabad, samples are then used for detailed microscopic studies for analyzing strain markers such as ooids and fossils etc. and calculating finite strain using Rf/φ methods (Ramsay, 196 ; Dunnet, 1969; Lisle, 1985) and Field studies were done along the bagnotar fault one of the major thrust. Along bagnotar fault for microscopic deformation analysis, ooids are recognized as strain markers in those thin sections and continuing fault line cretaceous exposed strata is also considered in current study because deformation has significantly deformed kawagarh formation by inducing fractures, for that Several strategies and procedures were available for data collecting. At the field, the scan line approach was employed to collect strike, using the Brenton Compass dip data is obtained. Structural determination data was accomplished by photo-geological interpretation. Rose diagrams and stereo net diagrams were utilized with recorded data from GeoRose Software for stress analysis and fracture inclination.

A total of twenty samples have been collected from oriented slabs of Jurassic age Samanasuk formation which are used for microscopic study such as tectonic induced strain that is used to determine the direction and magnitude of strain. Rocks during deformation undergoes various stresses and produce strain which could be translational, rotational, dilation, distortion. The strain is preserved in rocks as evidence and to measure the strain we need to recognize strain markers. These are the deformed features having known initial shape, they can be pebbles, fossils, lineation, reduction spots, ooids etc. (Pierre-Yves F. Robin, 1977), and Field studies were carried out along the 3-5km traverse of bagnotar fault where ooids and fold sets are recognized as strain markers. Strain analysis can be done manually by plotting fry on a set of tracing paper but in concerned study strain analysis of ooids is done by using ellipse fit 3. 9.1 software that is available at https://www.frederickvollmer.com/ellipsefit/index.html. After importing desired thin

section first of all we carefully mark the center particle point, initial fry plot will be a point in the center after that we mark all the ooids going outwards roughly in circles and then apply fry plot on those marked ooids applying fry plot will give an ellipse depending upon the ooids orientation and stress direction, after plotting we use Rf/ϕ method in this method ellipticity measure Rf, is plotted against orientation of long axis of object ϕ taking a reference direction e.g. north Rf is actually the ratio between the longer and shorter axis of deformed ooids it is the combination of ellipticity before strain Ri and strain ellipticity Rs (Waldron, 2016).. Fold sets are recognized as one of strain markers by comparing the shape before deformation or initial and after deformation or final shape of sequence and comparing initial and final lengths of folded sequence, strain in folding can be analyzed in 2D only. By keeping in view, the principle of original horizontality we can reconstruct the beds orientation before deformation. The figures 3.1 to 3.7 showing the stepwise details of the data put into the ellipse fit for the interpretation and results.

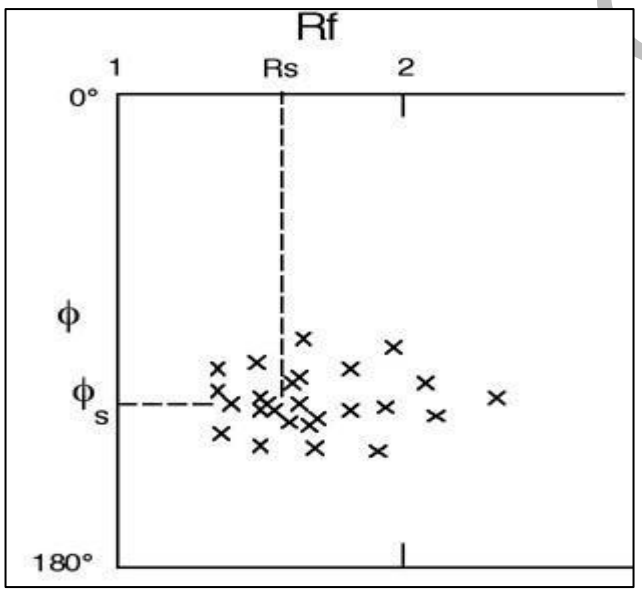

Figure 3-1: Showing the graphs with interrelationship of Rf = length/width and Rs corresponds by Rf tothe center of cluster points Available at: https://courses.eas.ualberta.ca/eas421/lecturepages/strain.html

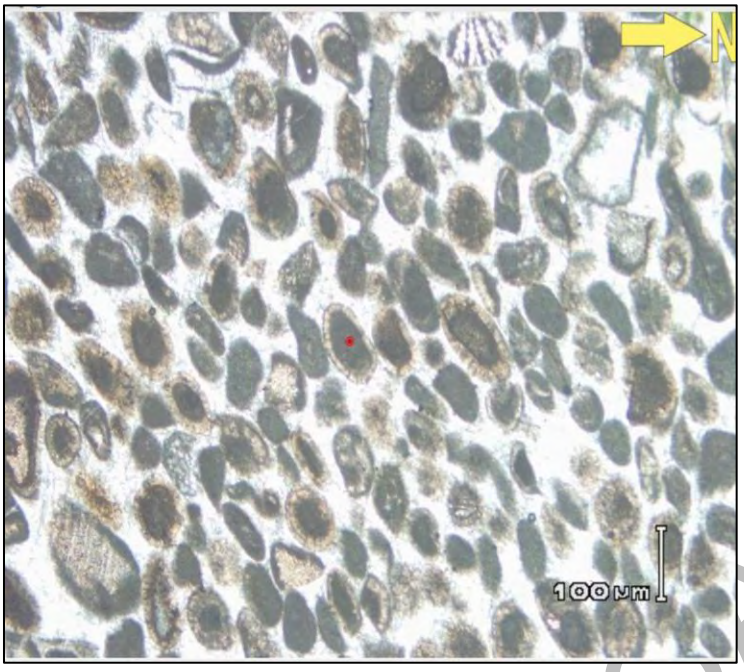

Figure 3-2: showing the first step of carefully marking the center particle point add tool and center point must be selected in the Ellipse fit software.

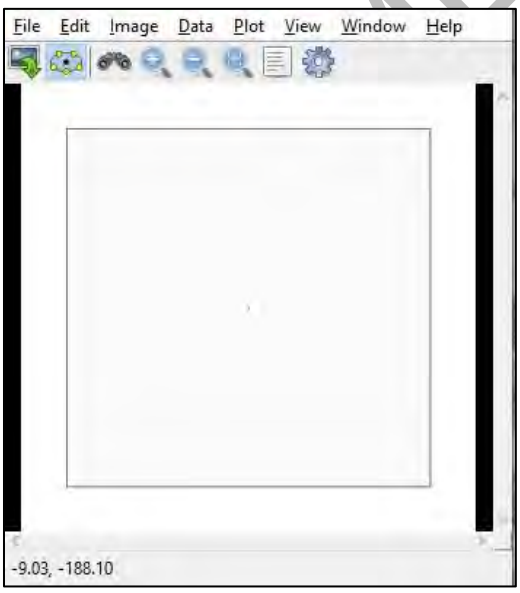

Figure 3-3: This step shows the Initially fry plot will be a point in a center Ellipse fit software

Figure 3-4: Continue digitizing all points roughly in a circular sequence not digitizing one ooid more than once if it happens then use cut" indicate as Red Cross in toolbox.

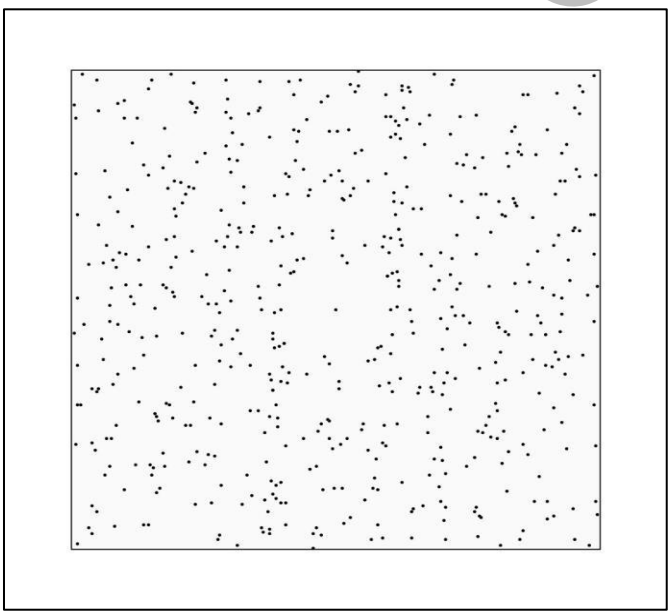

Figure 3-5: This step shows the applying the fry plot to get a centered ellipse and plot of marked ooids.

	ID	X	Y	Max	Min	Area	R	Phi
1	1	0.000	0.000	3.868	0.277	3.370	13.946	135.69
2	2	0.782	-0.165	6.691	0.178	3.751	37.494	26.80
3	3	1.890	-0.291	2.682	0.430	3.627	6.231	141.70
4	4	-0.293	1.746	3.609	0.266	3.020	13.548	163.42
5	5	-0.677	3.823	2.156	0.568	3.849	3.793	90.33
6	6	-0.408	-0.189	8.886	0.148	4.130	60.052	128.72
7	7	4.301	-1.811	2.324	0.502	3.666	4.628	23.66
8	8	1.409	-1.844	1.964	0.535	3.299	3.675	50.25
9	9	3.606	-4.640	2.930	0.250	2.305	11.704	72.26
10	10	-0.525	-1.160	2.365	0.346	2.570	6.835	7.19
11	11	1.099	-3.694	2.964	0.531	4.940	5.586	114.66
12	12	-0.353	-3.511	8.768	0.129	3.558	67.876	31.32
13	13	-2.994	-1.461	7.886	0.106	2.617	74.645	128.21
14	14	-1.196	0.480	4.287	0.253	3.402	16.969	36.43
15	15	2.232	1.371	3.818	0.252	3.028	15.122	89.74
16	16	-2.650	-2.212	6.108	0.160	3.073	38.130	139.77
17	18	-5.088	-2.296	2.209	0.555	3.849	3.984	93.44
18	19	3.859	1.149	1.981	0.572	3.562	3.461	68.57
19	20	-2.506	5.109	5.074	0.251	4.008	20.181	153.79
20	21	6.145	1.080	1.871	0.400	2.351	4.679	172.17
21	22	0.999	7.038	3.735	0.339	3.972	11.033	56.82
22	23	-1.827	5.650	8.006	0.103	2.594	77.626	28.49
23	24	-4.319	4.454	2.122	0.442	2.946	4.802	59.23
24	25	-6.293	0.659	2.396	0.285	2.145	8.407	157.48
25	26	5.011	-2.669	3.045	0.302	2.892	10.073	99.43
26	27	6.072	1.860	2.334	0.373	2.737	6.252	4.24

Figure 3-6: In the final step we will obtain Rf/ϕ by clicking at "Plot" and synthesis data table by clicking at "data-synthesize data."

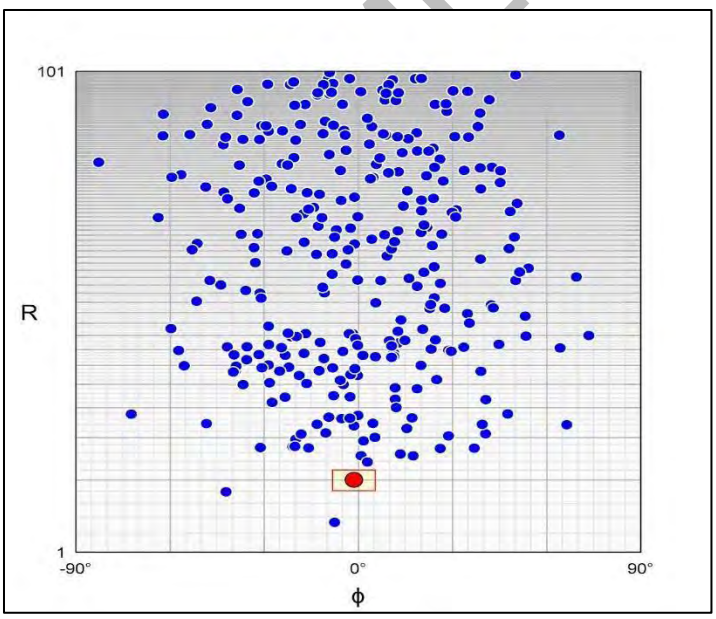

Figure 3-7: This setup displaying the R and phi data is plotted which was obtained from "synthesized data" Phi in degrees ranges from +90 to -90 such that the mean is reduced to 0 towards center. Blue points are representing Rf vs Phi and red point is showing mean orientation

We can understand morphotectonics of the area by knowing aspects such as geology, seismology and geochonological studies.

Fold sets are recognized as one of strain markers by comparing the shape before deformation or initial and after deformation or final shape of sequence and comparing initial and final lengths of folded sequence, strain in folding can be analysed in 2D only. By keeping in view the principle of original horizontality we can reconstruct the beds orientation before deformation

3.2 For stress analysis

We have conducted field studies in BaraGali area, Lesser Himalayas, Northern Pakistan. Many techniques were approached for collecting data. The scan line approach was employed for collecting data of fractures such as strike and dip via Brenton Compass, and exposure photos collected in the field. For st.ructural data determination, photo-geological interpretation was used. Rose and stereo-projections are utilised with GeoRose Software to analyse stresses and fracture orientation. Software of Illustrator and MS Work Sheet were used to create the illustration and calculation, respectively.

3.2.1 Scan line method

Scanline technique is an approach for recording brittle deformation such as jointing or fracturing data of an exposure for various analyses using this particular data. Simply drawing a projection of recorded measurement on concerned outcrop or strata was used in this manner. Then,all data that cross were recorded, including dip-strike, type of fracture, direction and angle , and an photograph of the exposure or lithology.

3.2.2 Data gathering

The dip-strike were recorded using a Brenton Compass, and the parameters of the research region were determined using a GPS device. The fracture length was determined using a portable tape measure. The images/photographs were taken with cell phones. To avoid any confusion in subsequent analysis, these data were entered in notebooks in a sequential manner, with naming each and every station at page top or headers

3.2.3 Work with Illustrations

Work with Illustrations As a result, we employ Adobe Illustrator, a software used for designing of graphics, to illustrate data containing some figures or tables or having rows or columns or photographs for better comprehension of data interpretation.

3.2.4 Software for Mapping

GeoRose Software was used to plot Strike and Dip data on Rose and Stereo net diagrams. These diagrams were used to compute various stresses and their directions, fractures dipping directions and their orientation, were mostly utilised for determining structure and area evaluation.

Chapter .4 Discussion and interpretation

4.1 Deformation and its stages

It is the resultant of applied stress on a rock body it varies as the amount and direction of stress varies it can be elastic or reversible which is the first stage of deformation in which stress and strain produced doesn't exceeds elastic limit of a rock body.(Ali M. Sadegh n.d.)

4.1.1 Stages

Deformation can be ductile as it only changes shape of body such as bending but it is permanent because of enough stress applied on a rock body after which rock cannot revert its original shape it is the second stage of deformation(Danielle 2019)Third stage is brittle deformation in which rock undergoes enough stress that strain produced in rock in the form of fractures or pieces.(Anon (March 28)) Folding is ductile deformation which is observed in samanasuk formation of Jurassic age which is exposed along bagnotar baragali section as the magnitude of stresses increases deformation exceeds maximum ductility limit and fractures are produced (Nelson) (Folding/Faulting: Topographic Expression of Folded Strata). Keeping stress and strain in relation we can understand deformation as show in Fig 4.1.

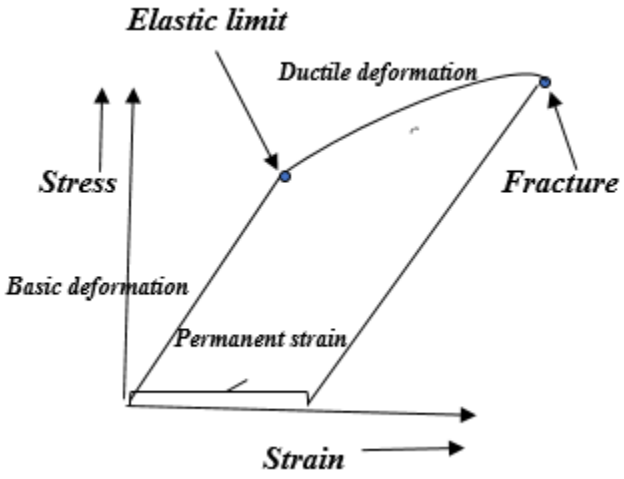

Figure 4-1: Showing the interrelationship of stress and strain accommodated in an area.

(Source: online; https://qsstudy.com/relation-stress-strain/)

4.2 Stress and strain

Stress applies movement to the rocks that causes strain, which is the resultant of stress applied, strain is non rigid deformation in which volume change may occur and may not occur(contributors 2023). Stress and strain are dependent on each other, stresses are applied, and particle displacement occurs which may result in dilation or distortion. Dilation is the change in size and distortion is the change occur in shape of rock. When we discuss strain analysis, we meant to analyze the aspects of deformation which involves measuring of strain orientation, strain magnitude and patterns of strain variation. Strain can be homogeneous or heterogeneous.(Danielle 2019) If a rock body undergoes same magnitude of stress so thus result in same amount of deformation in all directions, then it will be homogeneous strain lines do not get curved only change in orientation occurs and circles and spheres transform into ellipses and ellipsoid.(Anon 2023) If a rock body undergoes a different magnitude of stress so thus different amounts of deformation in all directions it is called heterogeneous strain lines get curved and circles and spheres transform into complex forms.(Anon n.d.-b)

4.2.1 Strain Analysis

Deformation of an object depends upon the size of object as well as stress applied on the object. When an object deforms it undergoes change in shape strain is measured in terms of extension which is change in length and area. (Kumar, Mahanty, and Chattopadhyay 2018)

(a) Strain ellipse

To determine finite strain of rocks having fabric that indicates history of deformation number of methods are available to analyze, by using change of shape of objects such as ooids and fossils one can determine the orientation and shape of strain ellipsoid or ellipse.(Anon n.d.-a) It is the 2D concept of measuring the angular and linear strain produced because of deformation of rock, the value of its radius is proportional to the stretch. Two principal axes are involved in strain ellipse; long axis or stretch axis, $1 + \varepsilon_1$ $\sqrt{\lambda_1} = S_1$ and short axis or shortening axis $1 + \varepsilon_3$ $\sqrt{\lambda_3} = S_3$ (Anon 2021)

Each strain point has two strain ellipses. An infinitesimal ellipse represents the strain at a single time point, whereas a finite strain ellipse represents the entire cumulative strain. The immediate direction of greatest strain and maximum contraction is the two-dimensional infinitely small strain axis. Consequently, among all known line orientations in the investigated timeframe, these are the lines with the quickest and weakest strain rates. In all cases, the strain axis is vertical.(JPB 2019)

(i) Shape

Ellipse shape is the ratio of longer and shorter principal axes, if we plot $1 + \varepsilon_1$ (x-axis) $1 + \varepsilon_3$ (y-axis) against each other, it shows the degree of distortion (Fig 4.2).

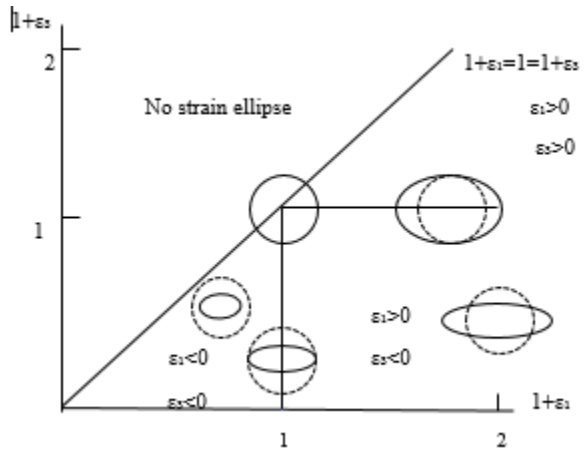

Figure 4-2: Showing change in ellipse shape with respect to principle axes

Scientific Figure on ResearchGate. Available from: https://www.researchgate.net/figure/Flinn-diagram-representing-three-dimensional-finite-strain-The-shape-changes-of-the_fig8_262974422

(ii) Area

Area of strain ellipse is the product of long and short principal axes. It is called dilatation. Its value will be positive if there is increase in area and will be negative if the area decreases as shown in the attached Fig 4.3.

$1+\Delta = (1+\varepsilon_1)(1+\varepsilon_3)$

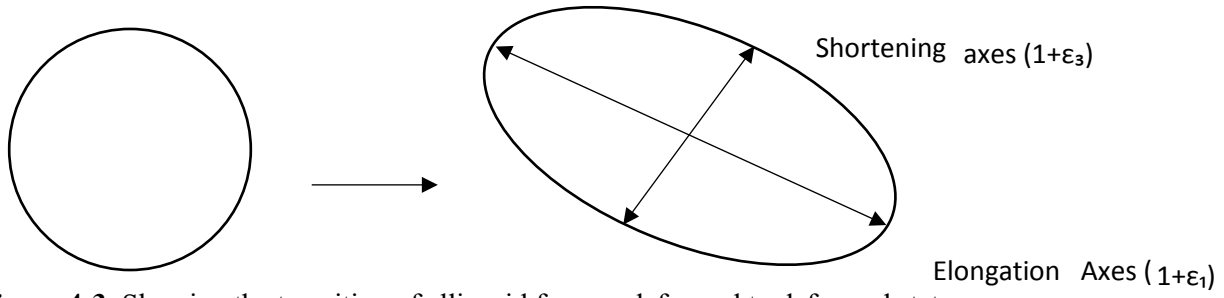

Figure 4-3: Showing the transition of ellipsoid from undeformed to deformed state

undeformed state homogeneously deformed state

Circle ⟶ ellipse

If we consider samples having deformed ooids collected from bagnotar thrust fault, shape of ellipse is determined by fry method developed by Fredrick Wolmer ellipse fit 3.9.1. We can analyze the magnitude of deformation of ooids from circle to ellipse by using fry plot in considered software and then plotting Rf/φ from the synthesized table from data of fry.

- **Rf/ ϕ analysis**

An analysis known as Rf/φ was performed on photographs of deformed elliptical Ooids using Ellipse Fit software. For all Ooids, we denote the lengths of the major and minor axes by l(fmax) and l(fmin), respectively, and record the orientation f of the major axis with respect to the baseline. Angles of orientation are considered positive clockwise and negative counterclockwise in the Rf/φ diagram. The stretch and its orientation determine the tendency and depression of the deformed ooid. The angular strain of Ooids across the bedding plane measured from the Rf/φ diagram should be subtracted from 90° to determine the immersion direction of the strained Ooids within the bedding plane. Positive and negative values are displayed on the right and left sides of the Rf/φ plot(Kumar, Srivastava, and Ojha 2014). The area of the deformed Ooid was calculated by multiplying the maximum and minimum strain axis lengths l (f-max) and l(f-min), respectively as shown in Fig 4.4.

4.2.2 Strain analysis of samples

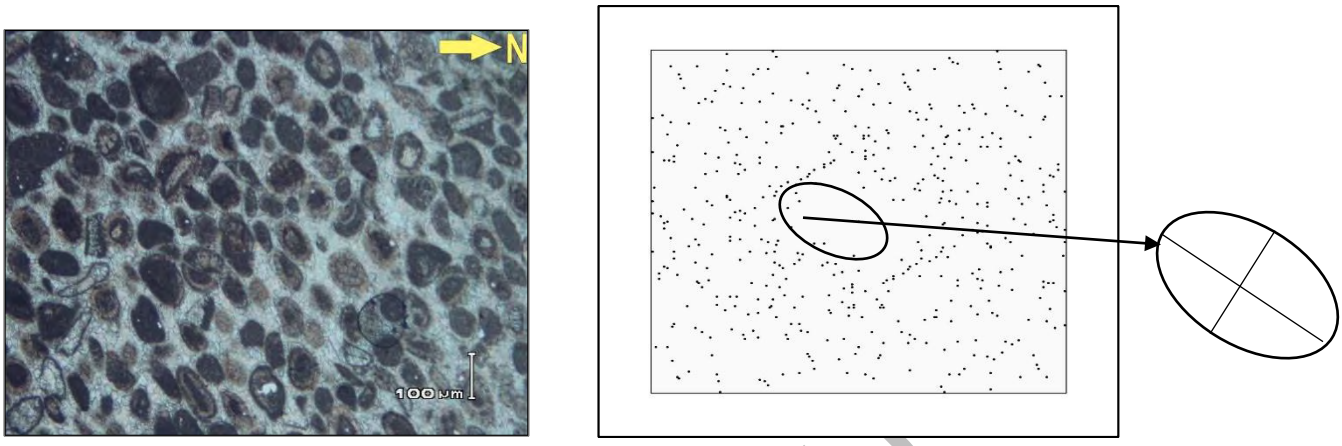

Figure 4-4: Showing the values of S_3=3.349, S_1=0.369 R_s 9.0 f 0 f or analyzed sample of ooids in Samanasuk Formation.

An oriented and digitized photomicrograph along the bedding plane of sample no S-23 (a) showing 66 deformed ooids having stretched maximum and minimum axial lengths mentioned in table1. Rs ratios are derived from axial lengths of ooids individually using https://www.frederickvollmer.com/ellipsefit/index.html by using fry plot an ellipsoid shape has been formed which longer and shorter principle axis can be calculated by taking average of longer and shorter principle axis of 66 deformed ooids. At x-axis along Ri, we have plotted graph and we get eight curves, with values (1.25, 1.5, 1.75, 2, 2.5, 3,4 and 6 respectively) while at y-axis they range from 90 to -90 in increments of 9. We get Ri (Lisle (1985) as shown in Fig 4.5 and Fig 4.6 respectively. The data set of the analyzed sample S-23 is given as under in the Table 4.1. This table contains both long and short axes, as well as the orientations, of up to 70 markers. Each strain marker's axial ratio (Rf) is determined, (Chew*, 29 (2003).

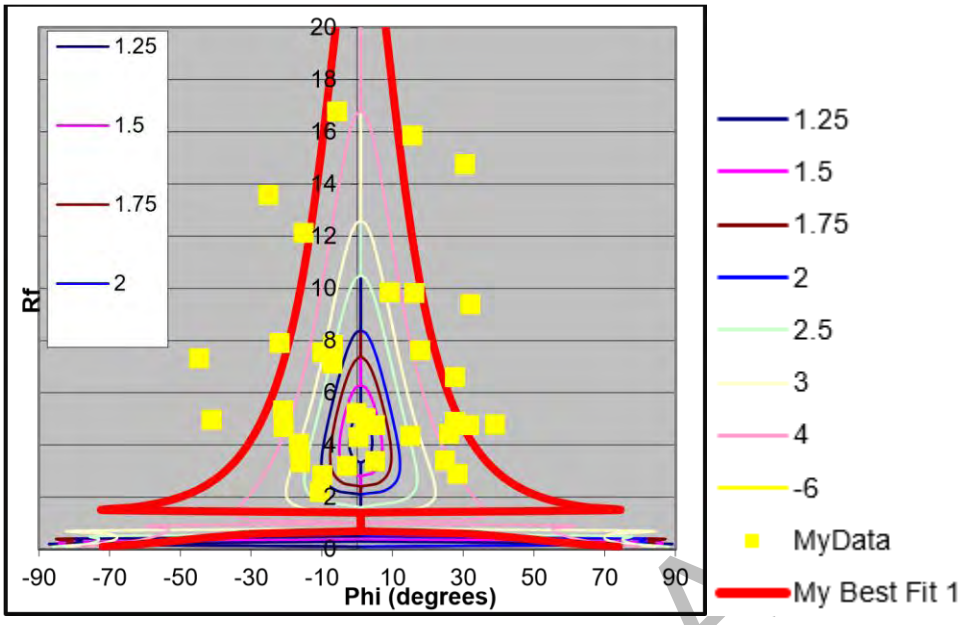

Figure 4-5: Presenting the X-Y plot of Phi Vs Rf values in each sample analyzed for ooids where red curve is showing best fit, yellow points are Rf vs φ points of ooids and different colours curves are representing different values of Rs

Table 4-1: Showing the collective data set interpreted in the ellipse fit for ooids data.

Max	Min	Phi	R	Max	Min	Phi	R
6.514	0.154	-11.29	42.429	2.187	0.457	38.93	4.784
2.765	0.362	17.93	7.643	1.827	0.547	-15.97	3.339
3.14	0.318	9.27	9.861	2.571	0.389	27.67	6.609
2.215	0.452	27.74	4.905	4.776	0.209	-2.26	22.813
4.965	0.201	-1.69	24.652	2.749	0.364	-9.75	7.556
2.086	0.479	15.1	4.352	4.997	0.2	24.99	24.967
1.488	0.672	-10.51	2.214	3.688	0.271	-25.06	13.602
2.182	0.458	31.61	4.762	6.119	0.163	-20.26	37.445
2.707	0.369	-44.7	7.329	1.409	0.71	10.77	1.986

2.668	0.375	-6.92	7.12	3.342	0.299	-17.61	11.172
2.308	0.433	-20.89	5.328	3.114	0.321	-28.61	9.697
3.844	0.26	30.61	14.774	2.122	0.471	40.8	4.503
2.288	0.437	-0.16	5.237	5.478	0.183	-3.28	30.004
1.839	0.544	5.08	3.383	2.463	0.406	-7.82	6.065
2.814	0.355	-21.9	7.92	2.642	0.378	32.63	6.981
3.065	0.326	31.95	9.391	6.379	0.157	-11.12	40.696
5.961	0.168	14.32	35.534	2.642	0.379	-11.44	6.978
7.913	0.126	-38.17	62.61	3.21	0.312	18.1	10.301
1.79	0.559	-2.9	3.205	4.188	0.239	-14.19	17.543
2.242	0.446	2.34	5.025	1.713	0.584	30.52	**4.934**

1.688	0.593	-9.87	2.848	3.597	0.278	2.63	12.936
2.8	0.357	-6.79	7.842	1.611	0.621	12.01	2.596
4.611	0.217	10.21	21.26	5.566	0.18	-12.63	30.983
3.483	0.287	-14.96	12.128	4.266	0.234	-32.88	18.201
3.137	0.319	16.1	9.84	1.577	0.634	18.65	2.487
2.076	0.482	0.37	4.308	2.688	0.372	9.38	7.223
2.231	0.448	-41.06	4.976	1.395	0.717	-0.12	1.945
4.098	0.244	-5.56	16.795	3.208	0.312	7.63	10.293
9.841	0.102	24.69	96.84	5.117	0.195	15.7	26.188
3.984	0.251	15.7	15.873	4.052	0.247	12.78	16.421
2.108	0.474	25.97	4.446	**3.349**	**0.396**	**1.759**	**9.07**
2.182	0.458	5.05	4.762				
1.846	0.542	24.92	3.408				
2.013	0.497	-16.45	4.054				
8.94	0.112	-35.23	79.918				
2.17	0.461	-20.68	4.709				
1.706	0.586	28.46	2.909				
2.187	0.457	38.93	4.784				
1.827	0.547	-15.97	3.339				
2.571	0.389	27.67	6.609				
4.776	0.209	-2.26	22.813				
2.749	0.364	-9.75	7.556				

- **Sample no 15**

Presenting the X-Y plot of Phi Vs Rf values for sample-15 analyzed for ooids. It is also showing the relevant thin section of strained ooids

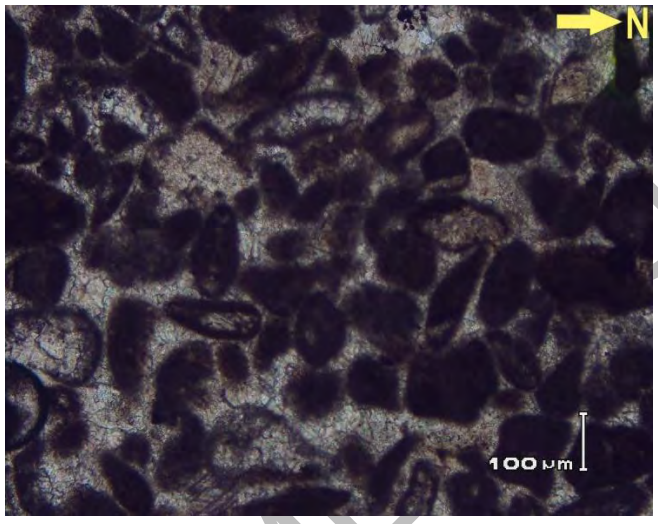

Figure 4-6: Showing thin section of field sample having strained ooid

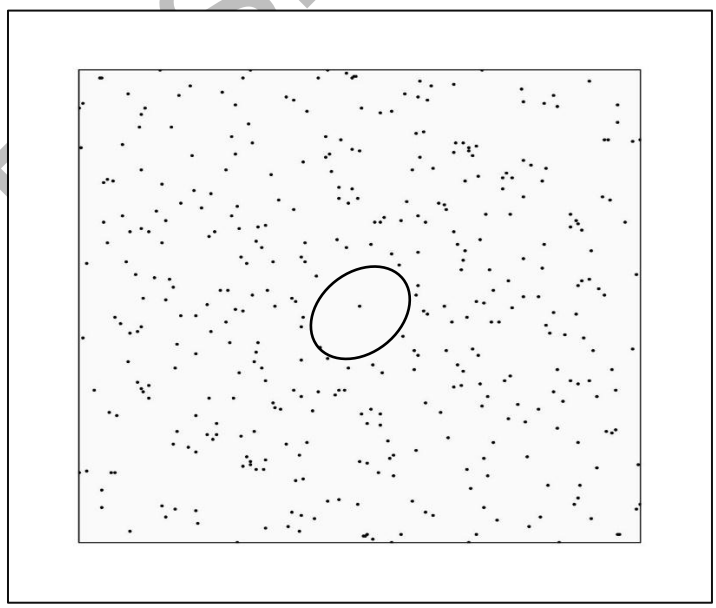

Figure 4-7: Showing fry plot obtained from ellipse fit of sample 15

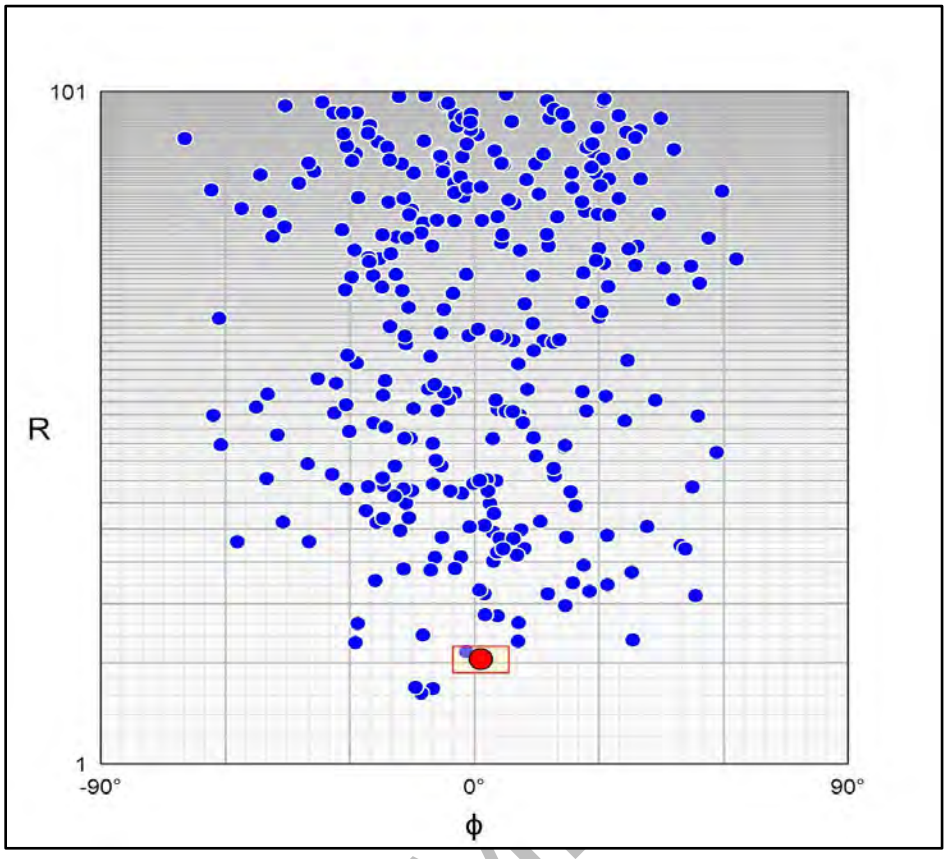

Figure 4-8: Showing Rf and ϕ values of sample 15

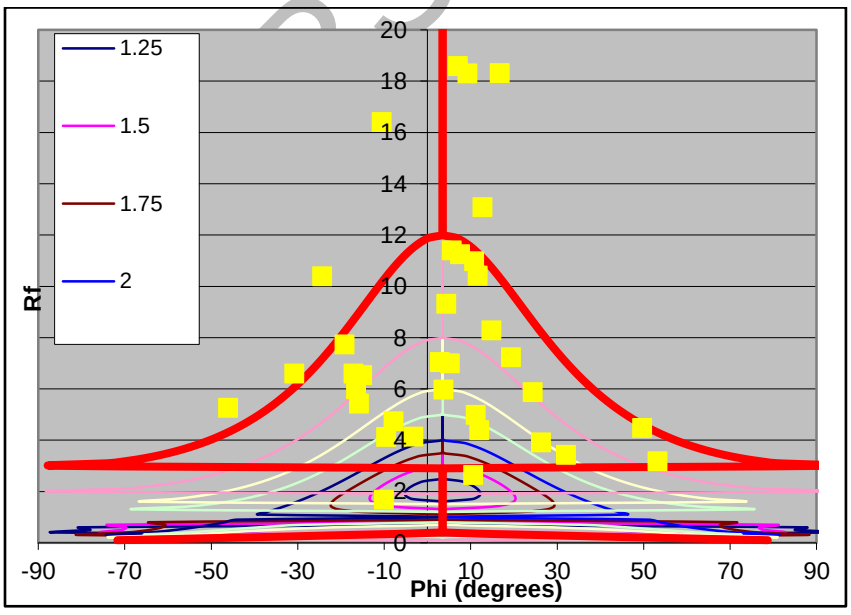

Figure 4-9: h owing Rf / ϕ curves along with Ri values encompassing points of best fit ellipse

- **Sample no 19**

  Presenting the X-Y plot of Phi Vs Rf values for sample-19 analyzed for ooids

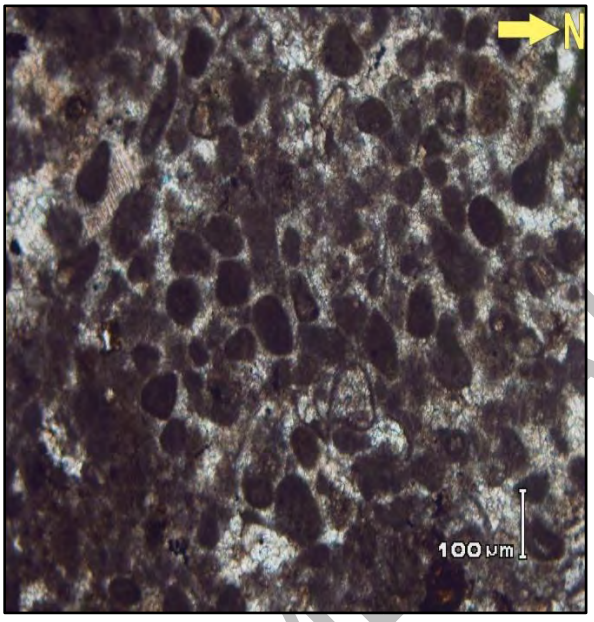

Figure 4-10: Showing thin section of field sample having strained ooid

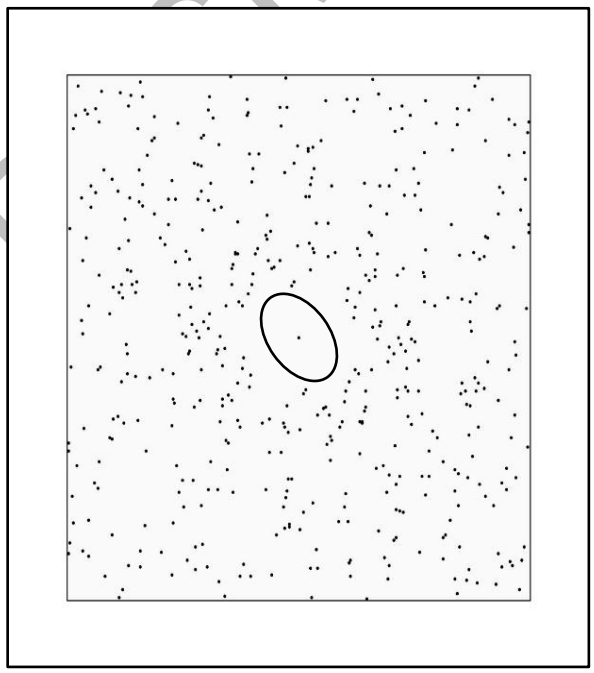

Figure 4-11: fry plot of sample 19 obtained from ellipse fit

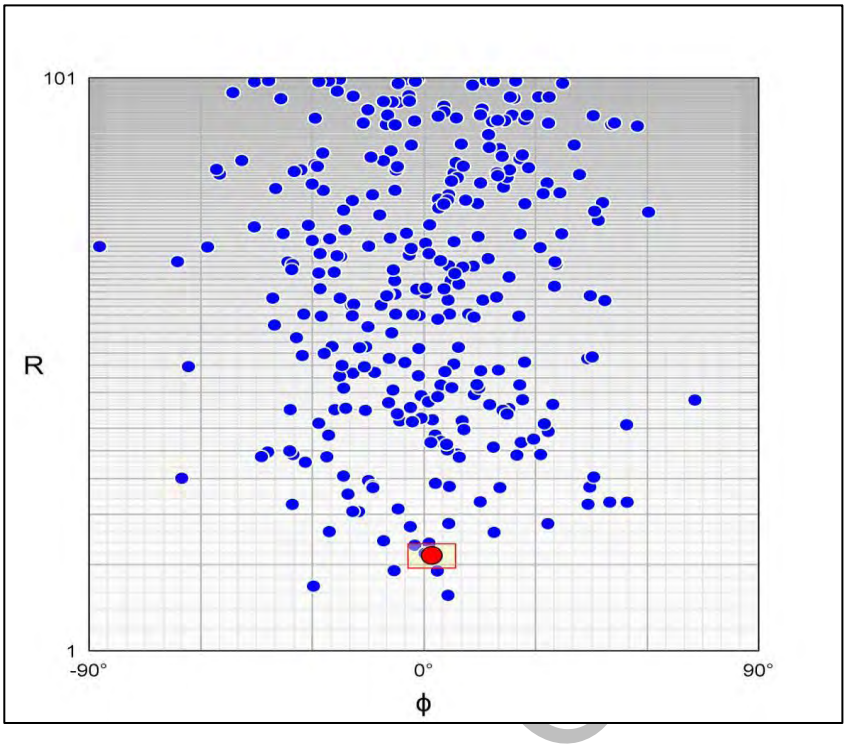

Figure 4-12: Showing Rf/ ϕ plot obtained from ellipse fit of sample 19

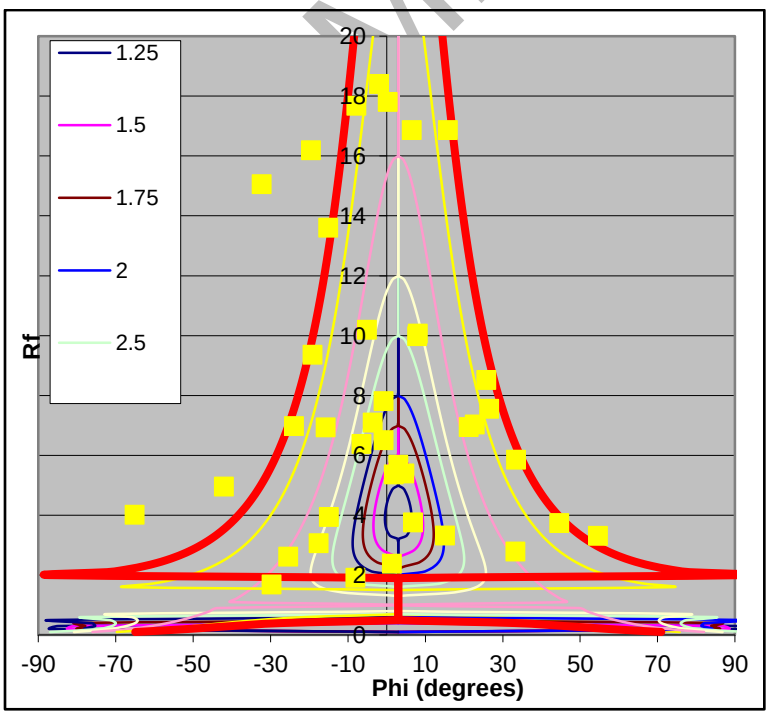

Figure 4-13: showing curves showing best fit point of ellipse along with Ri curve

- **Sample 20**

Presenting the X-Y plot of Phi Vs Rf values for sample-20 analyzed for ooids.

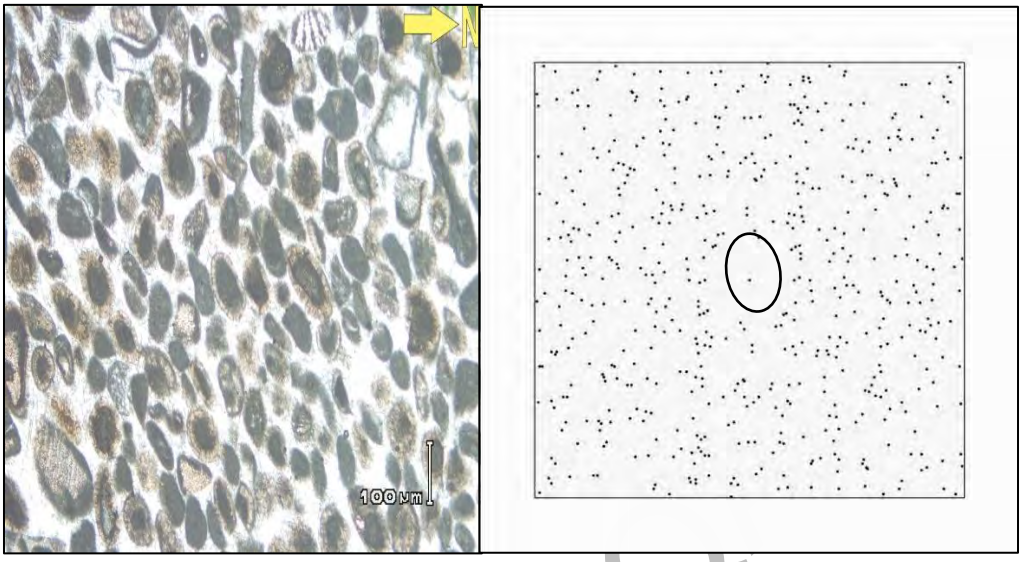

Figure 4-14 (a) presenting thin section of ooids **(b)** fry plot obtained from ellipse fit

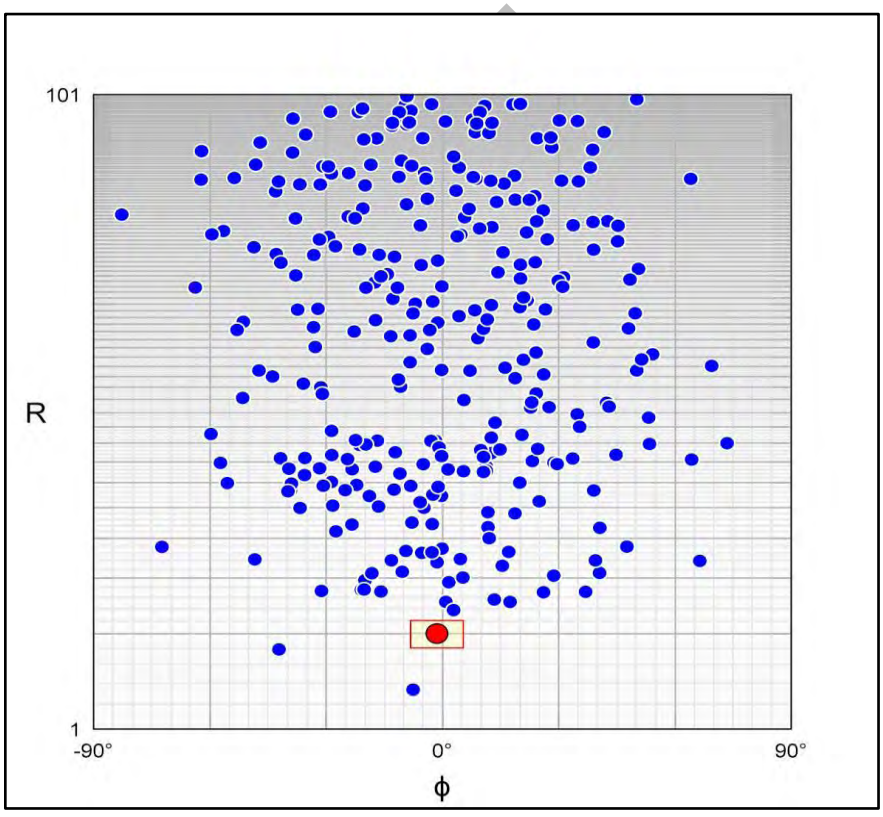

Figure 4-15: Showing Rf / ϕ plot of obtained from ellipse fit

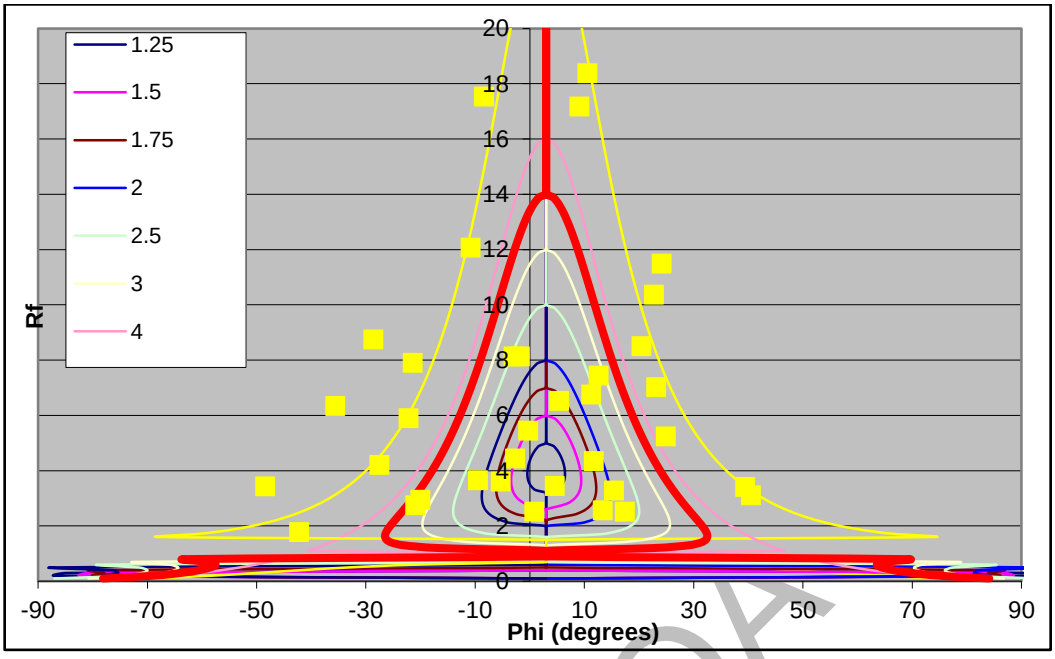

Figure 4-16: Showing curves showing best fit point of ellipse along with Ri curves

- **Sample no 23**

Presenting the X-Y plot of Phi Vs Rf values for sample-23 analyzed for ooids along with relevant thin section showing strained ooids

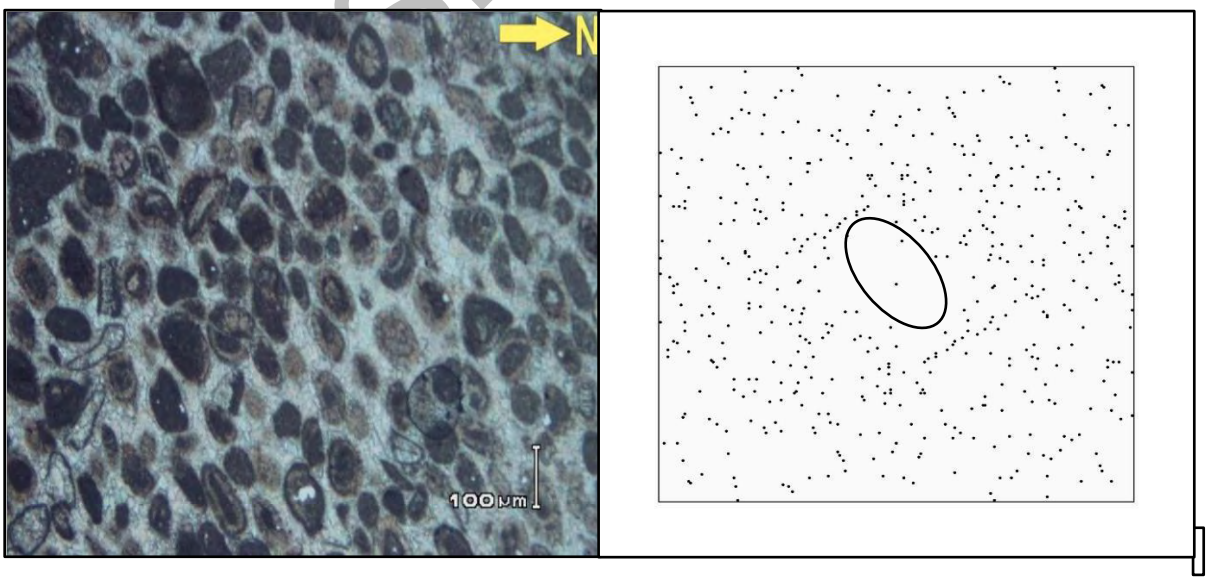

Figure 4-17: (a) showing thin section of field samle ooids **(b)** fry plot obtained from ellipse fit

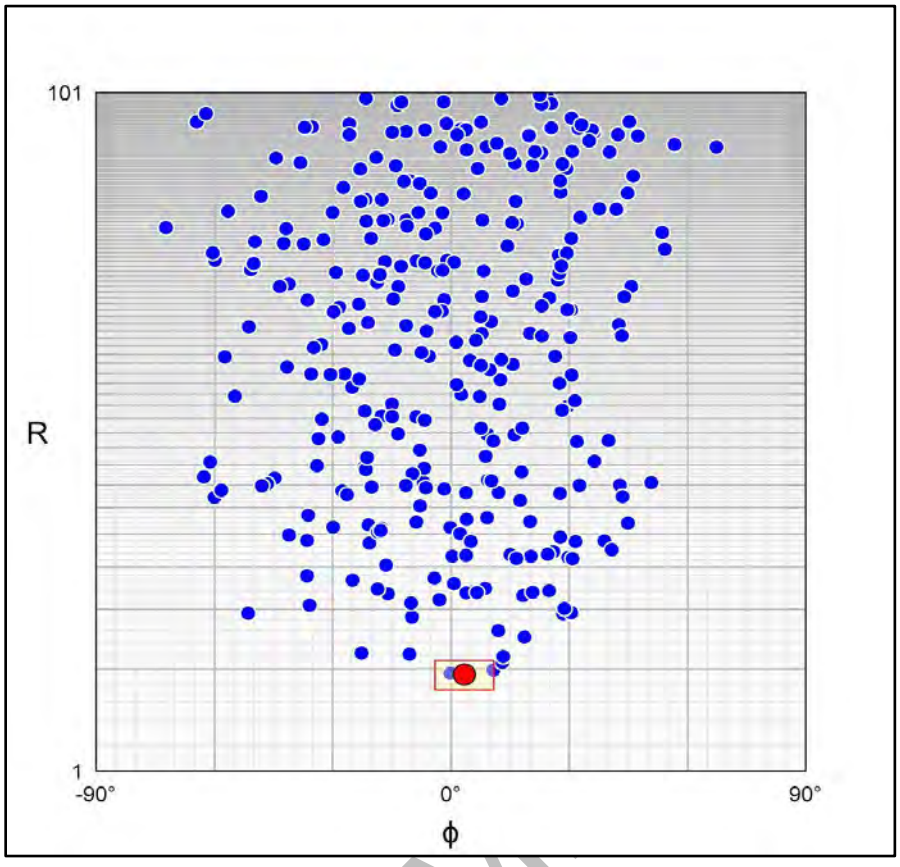

Figure 4-18: Showing Rf / ϕ plot obtained from ellipse fit

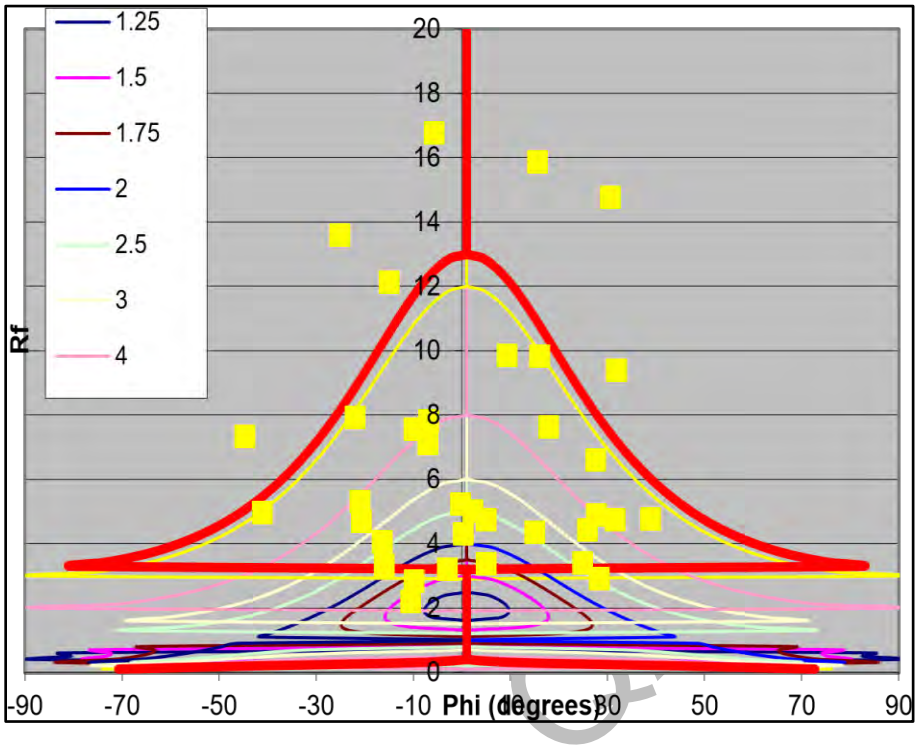

Figure 4-19: Showing curves showing best fit point of ellipse along with Ri curves

Table 4-2: Presenting the averages of marked samples ooids parameters Max, Min,Phi and R calculated from.

Sample no	Marked ooids	Phi (degrees)	R	Max	Min	Average shortening
S14	70	41	14.325	4.886	0.268	12.5
S15	57	26.95	12.612	3.176	0.380	16.8

S20	55	19.18	13.103	3.217	0.378	25.1
S19	47	18.81	9.143	2.854	0.3976	22.4
S22	80	29.5	14.965	3.318	0.383	22.2
S23	67	17.95	14.386	3.176	0.369	18.04
		25.6	**12.6**	**3.433**	**0.361**	**19.50**

Final ellipsoid is classified on the basis of averages are taken from minimum principal axes and maximum along with average of fluctuation in degrees from reference line of maximum principal axis mentioned in Table 4.2.

The initial form Ri is transformed to the measured final axial ratio, Rf. Ramsay and Lisle (1967) developed these changes analytically (1985). The Rf / technique computes the axial ratio of strain ellipse ellipticities (Rs). Rs = 1.0 in the undeformed condition. Rf and f values for a set of elliptical objects with varying beginning orientation but similar initial axial ratios (Ri) will plot inside an onion-shaped region, the shape of which is proportional to the axial ratio of the strain ellipse Rs. It should be noted that phi is measured about an arbitrary reference line. Changing this line shifts the plot along it but has no effect on the form of the area that surrounds the data points. The distorted long axes change by F on each side of the maximal extending direction. At the highest Rs levels, F becomes increasingly constrained. The fluctuation F signifies the range of position and direction of the elliptical object's long axes. With increased tension, the fluctuation reduces. At the highest value of Rf, the fluctuation curves for deformed strain indicators get closer.

Sample no	**Dispersion** Strain ellipse offset from current axis	**Theta** Pre strain orientation	**R_S** Stretch ellipse Ellipticity	**R_i** Initial Ellipticity
S-15	4	50	2.0	6.0
S-19	3.5	45	3.5	6.5
S-22	2	60	5.0	4.0
S-23	1	60	6.5	6.5
Averages	**2.6**	**53.7**	**4.2**	**5.7**

To differentiate the original shape and deformed strain indicator, the Rf approach may be used to quantify the strain amount of deformed strain markers. Graphs are invariably symmetrical along the long axis of the strain ellipse, and the points obtained from an originally randomly directed group of ellipses employed to gather around high Rf values on every curve (Ramsay and Huber, 1983). Oriented photomicrographs were obtained of samples collected along the bedding plane of the deformed ooids. On the R/Phi plots sections with minimum 50 and maximum 80 data points were shown. The strain ratio R and orientation f of the heavily deformed elliptical ooids are summarized in Table 4.1 and 4.2 The variations are fewer than 90 degrees. The region's strain ratios and angular strains are defined by a mean orientation 25.6^0 regarding true north (Table 4.1). Because of the size of the deformed ooids, fluid inclusions, pressure dissolving, and nonelliptical ooids, Rf/Phi data differ from sample to sample. Non-elliptical ooids were excluded from the study because they had sharp edges and irregular borders, and so make no sense with ellipticities. Because natural data frequently exhibit a significant spread due to changes in the morphologies and orientation to strain marker maximum shortening, the best fit curves of the R/Phi graph differ from Lisle's (1985) theoretical Rf/Phi graphs. Irregular curves are produced by randomly distributed ooids in oriented thin sections Figs 4.4 to 4.14 respectively. Negative shortening numbers were product 100 to obtain a variation in percentages. The maximum and minimum axial lengths of major axes of distorted ooids obtained by Ellipse Fit were restored to their original shape. To calculate the overall total shortening in all directed samples, the longer axes of every deformed elliptical ooid in directed

thin sections was averaged. Figure 4-20 illustrating the field images of folding in samanasuk formation of jurassic age clearly demonstrating a limb of folds in which stresses has produced strain at two different portions of same formation major shortening axis is marked with red. Pre strain ellipse theta, initial ellipticity R_i along with stretch ellipticity R_s and strain ellipse offset from current axis dispersion is shown in table 4.3

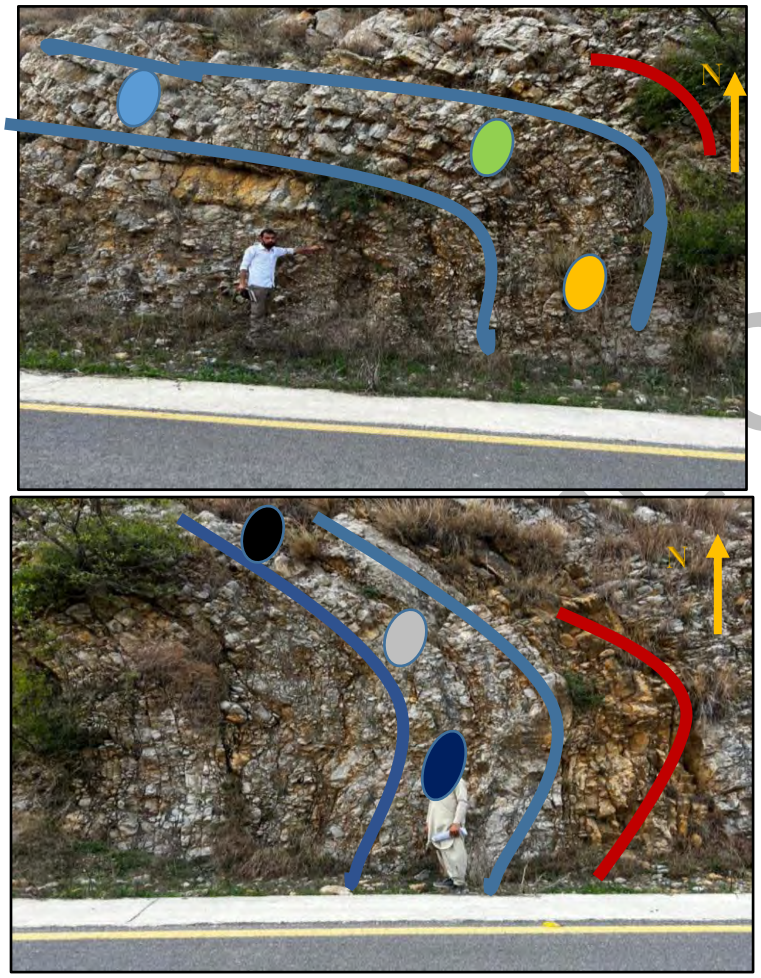

Figure 4-20: Field images of folding in samanasuk formation of jurassic age clearly showing a limb of folds in which stresses has produced strain at two different portions of same formation major shortening axis is marked with red. It is NW oriented strata in which camera is on South if we access this area from N35 it will be on western side along the road

Colour variations are showing samples from different places of folds in which green,grey and dark blue are showing sample numbers 20,22 and 23 and black ,blue and yellow is showing 14 15b and 19 respectively

Strike and dip data of fold altitude is

- N15W, 60NE
- N45W, 80NE
- N75W, 80NNE

4.3.1. Stress analysis

In this section, we looked at fracture's interpretation and data analysis. To evaluate the different characteristics of the fractures, we employed mathematical formulae and computations in an excel sheet. The fracture data was collected in the field at each site and represented in exposure images, as shown in Figure 4.24. A Rose Diagram was used to quantify and depict the stresses. The fracturing data for fractures that were intersected a specified line on the outcrop were recorded using the scanned line approach, as illustrated in Figure 4.21. Additionally, strike and dip statistics were gathered. The lengths and breadths of fractures for each site were again shown and determined using Illustrator. The rose diagram, which consists of circular pattern overlaid on radial segments (Anjum et al., 2022; Marshak and Mitra 1988), was employed to represent the information on fractures based on the reported scale. This resulted in a graphical and visual depiction of the fracture data. The rose diagram was created using the GeoRose program for the examination of the fracturing data acquired in the field. The stereo net models were employed to put the detailed geological on plane and lines for evaluation. The stereo net is made up of two sorts of circles: larger circles that pass through the center of the sphere and smaller circles that do not. The bigger circles represent longitude lines, whilst the smaller circles represent longitude lines on the globe. The position of the stereographic projection is specified by these big and small circles. In this work, we examined stresses and reservoir properties of the Kawagarh Formation, including the association between fracture density, fracture porosity, and fracture permeability. Himalayan Mountains Less than in the Galyat neighborhood near Bara Gali. The formation lies in northern Pakistan, which has been subjected to regional strain because of the convergence of the IndoEurasian plates, resulting in uplift, folding, and faulting. Based on fault data obtained at each station in the region, we employed a variety of methodologies and mathematical formulae to quantify stress and fault characteristics. Table 5-1 shows the results, which include the highest stress direction, the number of stresses per station, fracture density, fracture porosity, and fracture permeability. Furthermore, the stresses estimated using the Rose

diagram are shown on the geological map of the research region in Figure5. In this work, we estimated the stresses that are important in several domains, including structural geology, hydrogeology, engineering geology, basin modelling, and reservoir characterization. The estimates were based on fracture data acquired during fieldwork and evaluated using Rose. Diagram also with aid of GeoRose software.

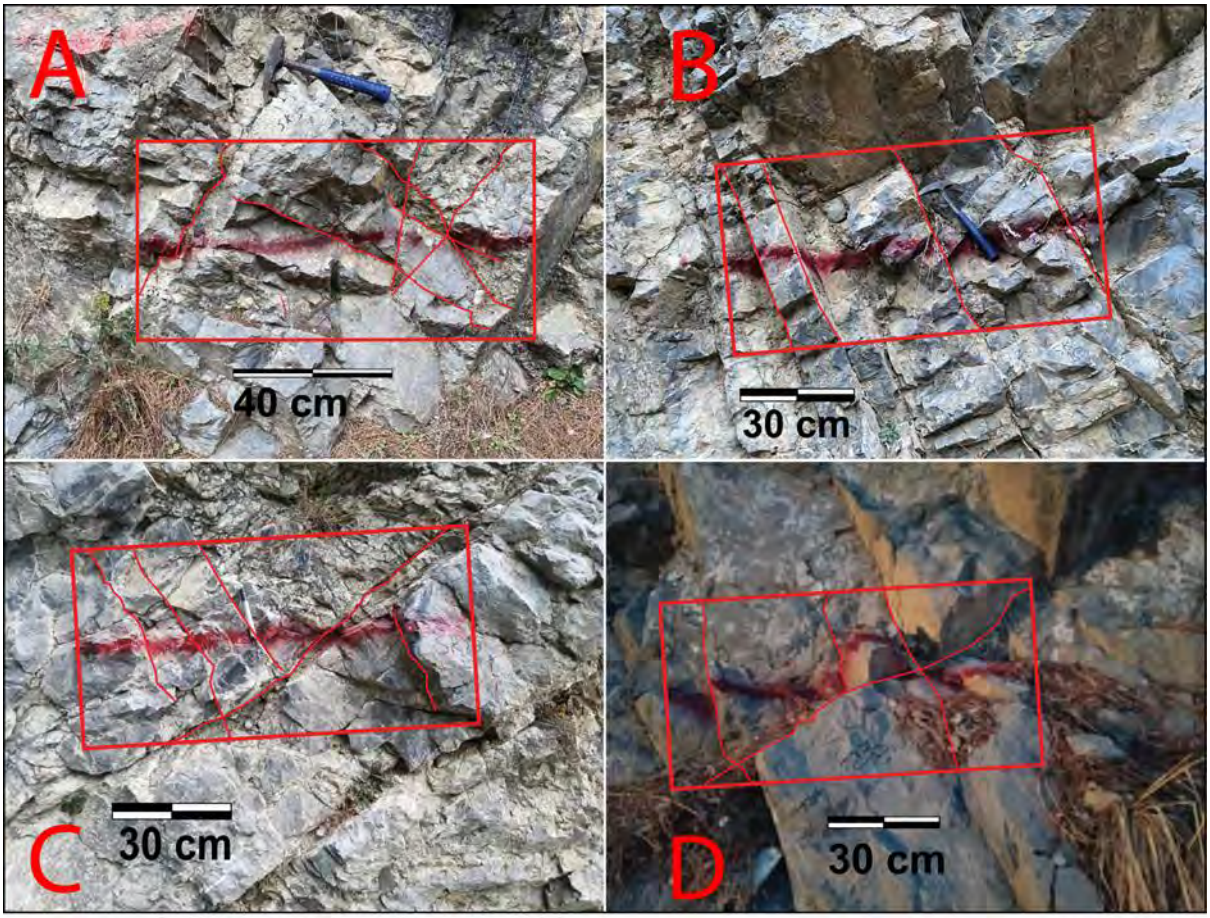

Figure 4-21: Showing Outcrops Fractures images taken during collecting of data at station 3,6,10 and 18 represented by A, B, C and D respectively. The Illustration was done for furthers Analysis.

- The investigation found that now the Kawagarh Formation is susceptible to three types of stresses, denoted by 1, 2, and 3 in Figure 4.15 (A). Forces or stresses are.
  - stresses direction(δ1)- NW- SE or maximum
  - stresses direction (δ)- NE-SW or intermediate
  - stresses direction (δ)- NEE-SWW or minimum

(a) NW-SE Oriented Stresses

Maximum stresses acting on the formation were found to be in the NW-SE direction in this investigation, as reported in 12 of the 18 locations. Sites 3, 4, 5, 6, 7, 8, 10, 11, 12, 13, 14, and 15 experienced these stressors. These stresses were projected on a Rose diagram and depicted on a Google Earth map of the research region as 1 in figures 4.24

(b) NE-SW Oriented stresses

Table 5-2 shows that 7 of the 18 stations exhibit strains in the Therefore among. These stresses, found at sites 1, 2, 3, 9, 16, 17, and 18, are categorized as intermediate stresses and are displayed on the Rose diagram. Fig .4.24 displayed on Google Earth of the research region, respectively. In both diagrams, these are marked by 2.

(c) NEE-SWW Oriented Stresses

The least stress operating on the research region, according to data collected at two stations, is the NEE-SWW orientation. These stresses, designated were plotted on the Rose Diagram and depicted on the Google Earth picture of the research region. Designated as 3 in figure.4-24.

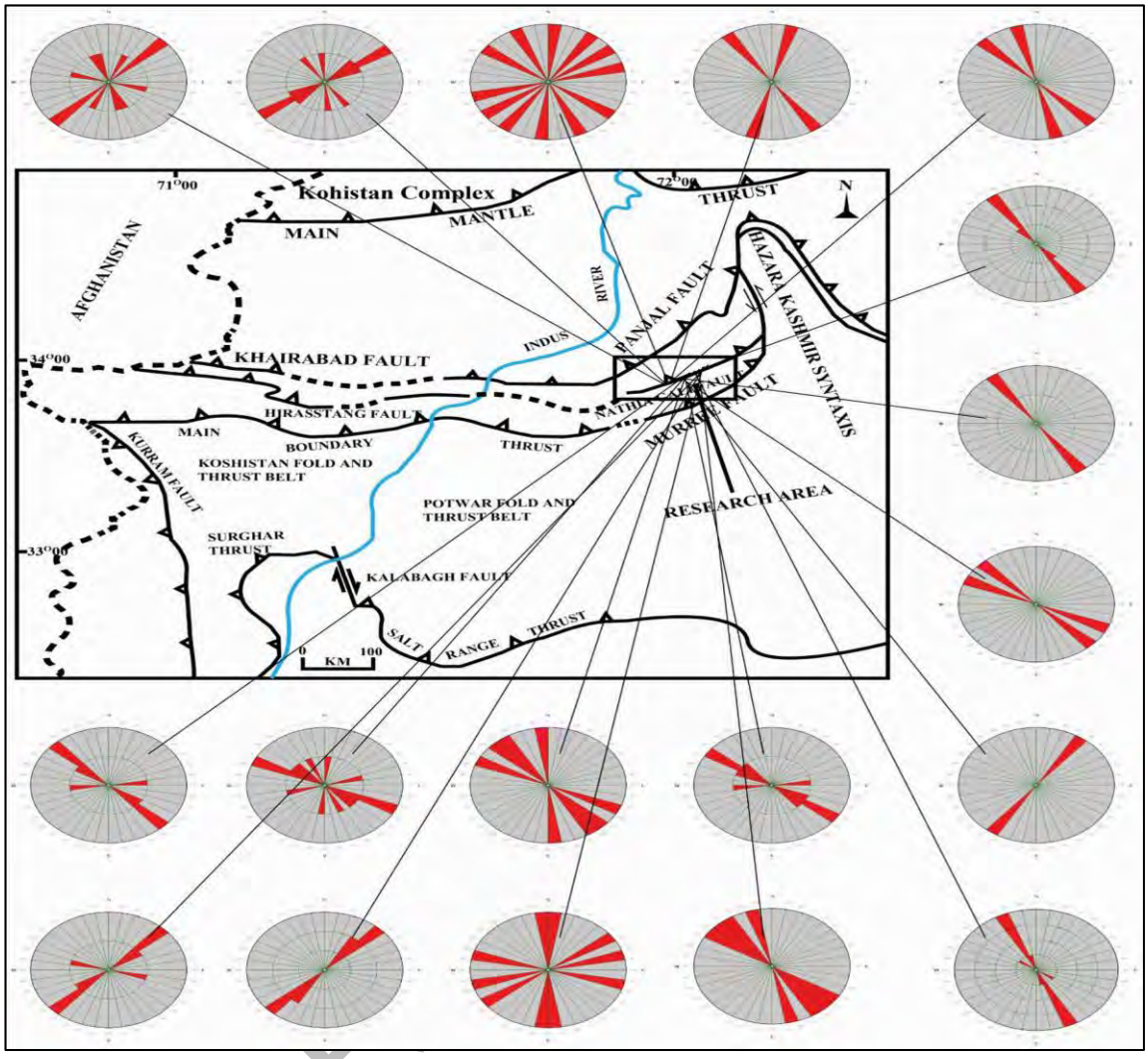

Figure 4-22: Showing calculated stresses on rose diagram of each station recorded at study area correlated with geological map of the study area.

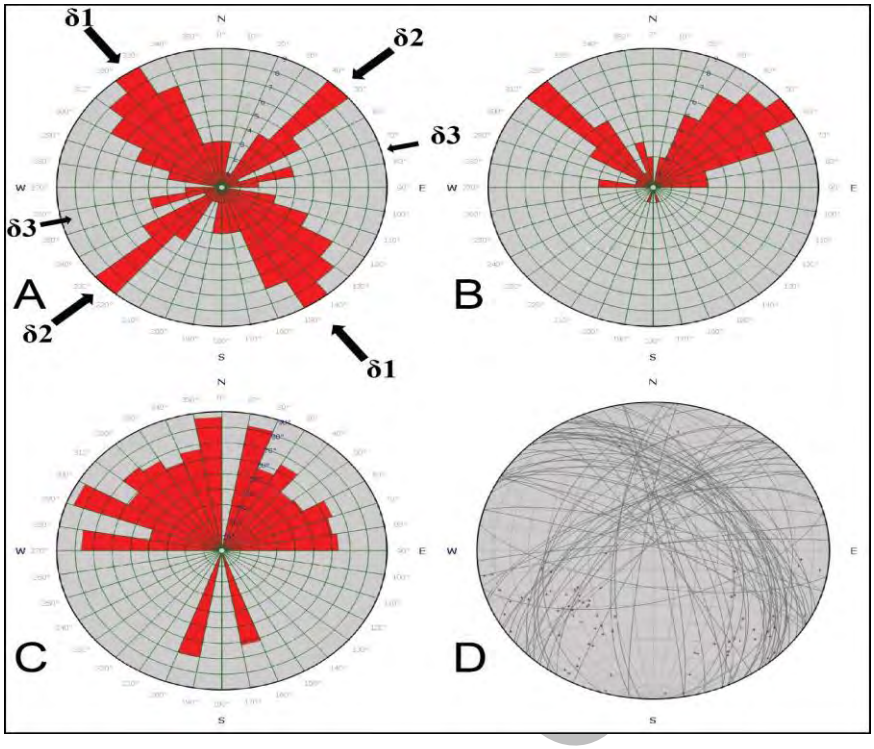

Figure 4-23:(A) Showing total fracture data recorded at field on different station. Also showing maximum stresses direction as δ1, intermediate stresses direction as δ and minimum stresses direction as δ . **(B)** Showing the dip direction data of fracture each station in a single rose diagram. **(C)** Showing dip angle data of all fractures on a rose diagram. **(D)** Showing over all data of fractures on a stereo net diagram.

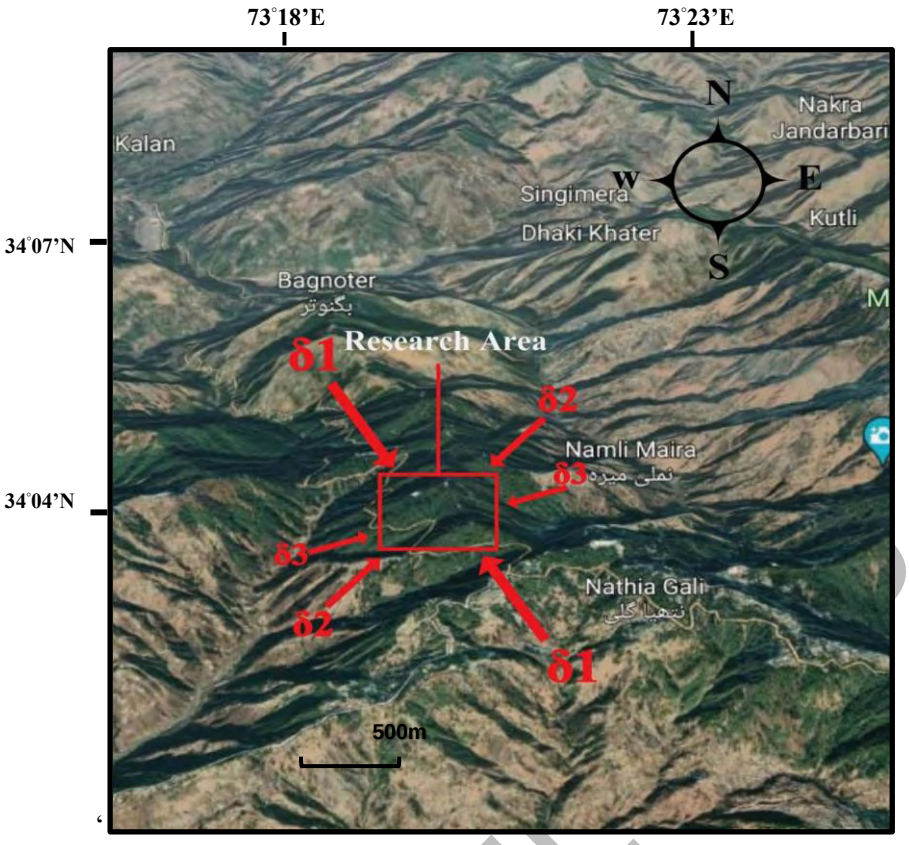

Figure 4-24: Showing the illustration of different stresses acting on the research area, where δ1 denotes maximum stresses and its direction, δ represents intermediate stresses and its direction, whereas δ shows minimum stresses and its direction.

4.3.2. Fracture Orientation

The strike and dip measurements acquired at each station during the field are used to determine fracture orientation. After analyzing all of the fractures, we found that the fractures are mostly directed in three directions: NW, NE, and NEE. As demonstrated in Figures 4.22 and 4.23 respectively, the maximum orientation of fractures is in the NW direction, the intermediate orientation is in the NE, and the minimum orientation is in the NEE direction. Figure 4.25 depicts fracture angles and directions using a Google Earth imagery.

Chapter .5 Results and Discussions

5.1 Strain analysis

5.1.1 Microscopic strain description

We must compile values obtained of strain analysis from ellipse fit software of samanasuk formation and compare with fractures analysis of cretaceous strata to get a correlation and regime of deformation of an area. Negative results of shortening were multiplied by 100 to obtain a percentage fluctuation. Elongation was determined by the difference between deformed and undeformed axial lengths divided by the undeformed dimension. The minimum and maximum axial lengths of the major axes of deformed ooids calculated by Ellipse Fit was returned to their original state (Ahmad, 2017). The ellipse shape, which was originally circular, is depicted by distorted elliptical ooids. It shows how spherical ooids may be distorted into ellptical ooids. The axes of circular ooids are approximately ~90 to the bedding plane in an undeformed condition, but the actual radii of the spherical ooids are not known. After stress, the circular ooids converted into elliptic nearly spherical ooids, now their axes are still not aligned somehow ~90 to with respect to the bedding.

Because the true size of the initial radius of the spherical ooids is not known and the fundamental strain values cannot be estimated directly, the ellipticity R and orientations f of the distorted elliptical ooids can be obtained. The ratio of the shorter principle axes and longer principle axial dimensions were measured and displayed on the graph for every elliptic ooid. As a result, the data computed from the distorted elliptical ooids along the bedding plane can provide a near simulation of mean ellipticity measure. Using the Rf/phi approach, the mean length of every principal semi axis was estimated from 6 oriented to bedding samples. Tables 4.1 and 4.2 were applied to calculate the final mean of maximum and minimum of the deformed elliptical ooids bedding parallel and vertical sections, which are described in table

4.3.3. Regional macroscopic strain description

The process underlying the early formation of the HKS, which is curved it towards foreland and convex to the primary transport, was a transition in regional transport pattern from

southward to southeast (Bossart et al., 1988). Most regional stresses, along with the Khairabad/Panjal, Bagnotar, Hissartang/Nathiagali, and MBT faults, are truncated along the sinistral shear zone, which was created because of unequal stresses caused by the HKS's subsequent anticlockwise movement. On a regional scale, continuing anticlockwise rotation generated southeastward movement for the Panjal, Nathia Gali, and MBT faults across the western extremity of the HKS. In the terminal part of the Hazara Kashmir Syntaxis near Balakot, a shear zone with sinistral shear regime exists (cf. Bossart et al., 1988, 1989). Likewise, Coward et al. (1986) used stretch slope of the line in the northwestern orientation of the HKS to restrict the southeastward relative stresses of the regional thrusts. The northwestward displacement of paleomagnetism maintained in Lower and Upper Cenozoic molasse sediment in the Potwar Basin, which deduced from the Himalayas just after foremost collision ofndian Plate and the Kohistan Island Arc, provides very significant proof that the stratas on the western side are older than the stratas on the eastern side. The HKS are spun anticlockwise in a manner that differs from the Indian Plate's major tectonic transit (Opdyke et al., 1982). Furthermore, this anticlockwise movement may be observed in the manner of sinistral shear context to be connected to the macro, meso, and micro components on the western part of the HKS. The HKS's anticlockwise revolution caused thick-skinned tectonics in the manner of overturn folding stratas and NW-verging sinistral shear zones (Fig. 3). steep dipping front thrusts and related back thrusts created pop-up features in the Bagnotar and Nathiagali Thrusts deformation thrust sheets (Fig. 3). The Jhelum strike slip fault runs NNW-SSE and is a significant sinistral strike slip shear zone (DiPietro and Pogue, 2004; Bossart et al., 1988; Calkin et al., 1975). It is regarded as the syntaxial zone's youngest tectonic event since it terminates the eastward extensiof MBTMBT, Nathiagali, and Panjal Thrust faults (Kazmi and Jan, 1997). The sinistral regime is connected to the HKS's ultimate anticlockwise revolution.

4.3.4. Microscopic-macroscopic strain comparison

Direction of deformed elliptic ooids observed in the Samana Suk Formation represents the region's stacked tectonic processes. The Rf/Phi model is used to determine the modification of bedding horizontal and vertically damaged elliptical ooids. The bedding parallel deformed elliptical ooids trends were created using the true north as reference. Microscopic to mesoscopic

structural shortening are parallel to the local tectonic fabric. These structures' subsequent NW vergence suggests anticlockwise rotation and WNW—ESE asymmetrical stress with shear sense around a major NNE—SSW developing component axis. Paleomagnetic studies by Opdyke et al. (1982) suggest the HKS and the rocks found on its western side rotating anticlockwise.

4.4. Stress analysis

The focus of this study was to analyze the fractures in the Kawagarh Formation located in the Galyat Area of the Lesser Himalayan region in Northern Pakistan. The researchers collected data from 18 stations, which included 75 fractures, and used the information to assess the stress and reservoir potential of the Kawagarh Formation in the study area. The results of the study revealed the following information about the fractures in the Kawagarh Formation. The major stresses acting on the formation are NW-SE directed.

- The intermediate stresses acting on the formation are NE-SW directed.
- NEE-SWW directed stresses are minor stresses acting on the formation.
- Most of the fractures are oriented in NW-SE direction.
- A moderate number of fractures are oriented in NE-SW direction.
- The least number of fractures are oriented in NEE-SWW direction.

4.4.1. Comparison of stress and strain analysis

In a study of stress analysis based on fractures of the Cretaceous formation, the results showed that the maximum stress direction was in the NW- E direction or δ1. This finding was in line with the results of the micro-meso and macroscopic strain analysis conducted by Yaseen (2022). Another study of strain analysis on the Samanasuk formation by Ahmad, October. (2017) found that the major stress direction was in the NW direction and was regionally oriented. The corresponding folding samples had ooids as strain markers.

4.5. Conclusions and Recommendations

The following conclusions are deduced from the current research work.

- Direction of deformed elliptic ooids observed in the Samana Suk Formation represents the region's stacked tectonic processes. The Rf/Phi model plot is helpful in determining the modification of bedding horizontally and vertically damaged elliptical ooids.
- Microscopic to mesoscopic structural shortening are parallel to the local tectonic fabric.
- The intermediate stresses acting on the formation are NE-SW directed. The NEE-SWW directed stresses are minor stresses acting on the formation. While majority of the fractures are oriented in NW-SE direction, while minimal number of fractures are oriented in NE-SW direction.
- So overall major stress directions are in NW-SE direction increasing deformation is in NW direction with principle stretching axis is at right angle to shortening which is WNW-ESE
- Average negative shortening is approximately 19.50% with maximum shortening was indicated as 25.1% and minimum at limb 12.5%
- By looking at the tectonic regime of area events of deformation seems to be occurring at same time of Indo-Eurasian collision but the intensity increases as we move from SamanaSuk Formation to the Kawagarh Formation
- Folding is ductile deformation which is observed in samanasuk formation of Jurassic age which is exposed along bagnotar baragali section as the magnitude of stresses increases deformation exceeds maximum ductility limit and fractures are produced.
- Analysed samples can be correlated with a balanced cross section to interpret the regional direction of paleo stresses which will provide a significant understanding of mechanisms involved such as crustal uplifting, subsidence or folding, faulting resulting in alteration of morphology along bagnotar fault
- The distribution of paleostresses and ooids substiates a tectonic regime due to far-field Himalayan compression and a lateral escape component of the allochthonous fold-and-thrust-belt away from the growing bagnotar fault possibly.
- Timing events need to be very generalized in our limited data

- Furthermore history can be determine by using integrated studies approach including a data of vast area along with gravity and magnetic data which need to elaborate further in another study

Table 5-1: showing details of all fractures recorded on each station.

Station no	Formation name	Total no of fractures	Calculated maximum stress direction	Fracture density in cm^{-1}	Fracture porosity in %	Fracture permeability in Darcy
1	Kawagarh	6	NE	0.056579	5.744593	0.62465328
2	Kawagarh	6	NE	0.052556	2.409913	0.036198527
3	Kawagarh	6	NW,N,NE, NEE	0.059631	1.423724	0.003170242
4	Kawagarh	2	NW, NNE	0.030796	3.596382	0.282737557
5	Kawagarh	2	NW,NNW	0.029183	1.72971	0.043774525
6	Kawagarh	4	NW	0.041698	1.227604	0.00388027
7	Kawagarh	2	NW	0.020542	2.694956	0.230211941
8	Kawagarh	2	NW	0.019395	5.605357	1.744858958
9	Kawagarh	1	NE	0.010039	1.234824	0.065385786
10	Kawagarh	5	NW	0.052563	2.729485	0.072694951
11	Kawagarh	4	NW, N	0.043057	6.323399	0.768554861
12	Kawagarh	7	NW	0.075705	4.915553	0.131278765
13	Kawagarh	4	NW	0.03462	4.861405	0.576116111
14	Kawagarh	6	NW	0.064841	3.474358	0.094008338
15	Kawagarh	4	NW, NNW	0.036907	0.918661	0.002658363
16	Kawagarh	5	N,NWW, NE,NEE	0.049819	3.614183	0.315167804
17	Kawagarh	5	NE	0.050392	2.835621	0.059664358
18	Kawagarh	4	NE	0.04812	2.48543	0.026359065

Sample no 14

Table 5-2: Showing sample no 14

ID	X	Y	Max	Min	Area
1	0	0	1.703	0	3.142
2	-0.336	-0.874	3.349	#NAME?	3.142
3	-0.735	1.026	4.554	0.22	3.142
4	0.349	1.462	2.234	0.448	3.142
5	-2.366	2.524	1.796	0.557	3.142
6	-3.913	3.14	3.819	0.262	3.142
7	-1.27	3.284	2.526	0.396	3.142
8	-4.167	0.608	3.015	0.332	3.142
9	1.209	3.339	7.675	0.13	3.142
10	0.317	4.94	3.697	0.271	3.142
11	1.401	-1.204	2.858	0.35	3.142
12	5.392	-0.958	2.137	0.468	3.142
13	-0.203	-1.983	1.851	0.54	3.142
14	-4.557	3.476	2.967	0.337	3.142
15	4.965	-1.915	2.336	0.428	3.142
16	-7.398	1.233	1.522	0.657	3.142
17	-1.581	3.966	4.437	0.225	3.142
18	5.289	0.097	2.392	0.418	3.142

19	7.455	-2.725	2.925	0.342	3.142
20	3.917	3.347	2.161	0.463	3.142
21	-7.558	4.63	4.177	0.239	3.142
22	4.129	1.304	1.9	0.526	3.142
23	8.74	0.303	3.402	0.294	3.142
24	12.572	-3.473	2.344	0.427	3.142
25	-0.479	5.935	1.836	0.545	3.142
26	4.68	-2.953	1.809	0.553	3.142
27	7.387	-3.415	7.363	0.136	3.142
28	3.703	4.282	2.417	0.414	3.142
29	6.702	4.64	2.112	0.473	3.142
30	0.058	-3.15	2.291	0.436	3.142
31	7.403	-3.997	2.258	0.443	3.142
32	-1.241	7.009	3.534	0.283	3.142
33	-5.485	4.974	2.756	0.363	3.142
34	-4.109	5.514	5.474	0.183	3.142
35	-10.672	1.657	3.375	0.296	3.142
36	12.303	-4.512	2.205	0.454	3.142
37	-9.486	5.163	2.731	0.366	3.142
38	2.471	-3.655	2.434	0.411	3.142
39	-4.338	-0.976	3.045	0.328	3.142

40	-1.131	-2.57	5.359	0.187	3.142
41	-4.16	7.869	1.978	0.506	3.142
42	10.711	-5.967	3.548	0.282	3.142
43	-0.364	-4.466	1.891	0.529	3.142
44	3.269	6.174	8.627	0.116	3.142
45	0.564	7.611	1.77	0.565	3.142
46	-3.136	8.779	2.581	0.387	3.142
47	2.392	9.028	1.913	0.523	3.142
48	10.116	0.965	2.115	0.473	3.142
49	5.522	-5.47	2.033	0.492	3.142
50	1.679	10.478	1.428	0.701	3.142
51	6.727	5.569	2.254	0.444	3.142
52	-1.007	-5.475	3.745	0.267	3.142
53	-3.633	9.718	2.187	0.457	3.142
54	-6.778	9.622	4.305	0.232	3.142
55	-5.287	-2.085	5.508	0.182	3.142
56	3.541	6.745	2.352	0.425	3.142
57	6.206	7.089	3.757	0.266	3.142
58	-1.136	-6.252	1.954	0.512	3.142
59	3.16	11.817	2.187	0.457	3.142
60	7.691	8.33	4.128	0.242	3.142

61	-4.604	-6.346	3.005	0.333	3.142
62	-3.951	-6.903	8.407	0.119	3.142
63	-2.526	-7.115	4.193	0.238	3.142

- **Sample no 19**

Table 5-3: showing sample no 19

ID	X	Y	Max	Min	Area
1	0	0	2.536	0.394	3.142
2	0.871	-0.585	2.918	0.343	3.142
3	0.138	0.821	2.384	0.42	3.142
4	-3.005	0.772	2.749	0.364	3.142
5	1.309	1.853	1.543	0.648	3.142
6	4.901	2.71	3.16	0.316	3.142
7	-1.514	2.077	4.508	0.222	3.142
8	0.122	3.06	3.059	0.327	3.142
9	-4.386	1.587	1.381	0.724	3.142
10	-3.455	-1.354	2.652	0.377	3.142
11	1.208	3.435	4.58	0.218	3.142
12	2.237	-0.687	4.106	0.244	3.142
13	-6.87	-1.043	1.668	0.599	3.142
14	2.845	-1.225	3.194	0.313	3.142

15	3.645	4.407	1.822	0.549	3.142
16	5.133	1.029	4.106	0.244	3.142
17	-0.699	4.775	2.794	0.358	3.142
18	0.962	-1.592	2.227	0.449	3.142
19	-0.151	5.657	1.616	0.619	3.142
20	7.37	5.114	2.324	0.43	3.142
21	-1.304	6.931	2.552	0.392	3.142
22	3.681	5.698	1.933	0.517	3.142
23	3.053	-3.41	1.819	0.55	3.142
24	0.025	-1.752	3.88	0.258	3.142
25	5.664	-0.418	2.315	0.432	3.142
26	-6.068	2.592	2.664	0.375	3.142
27	-6.754	-2.873	2.004	0.499	3.142
28	-1.392	-2.187	4.715	0.212	3.142
29	-11.86	-1.159	4.219	0.237	3.142
30	0.193	7.431	3.688	0.271	3.142
31	-7.117	-0.132	3.173	0.315	3.142
32	9.899	2.593	4.925	0.203	3.142
33	9.244	0.76	2.634	0.38	3.142
34	8.241	-0.993	1.938	0.516	3.142
35	5.201	7.4	2.641	0.379	3.142

36	11.306	-0.626	1.985	0.504	3.142
37	0.228	-3.291	4.205	0.238	3.142
38	-1.769	8.314	4.29	0.233	3.142
39	4.733	-2.761	1.297	0.771	3.142
40	7.415	-1.99	2.634	0.38	3.142
41	-8.953	-3.022	2.525	0.396	3.142
42	-4.2	5.289	1.751	0.571	3.142
43	-10.858	0.039	2.419	0.413	3.142
44	0.978	-3.991	4.024	0.249	3.142
45	-2.328	8.96	4.139	0.242	3.142
46	6.358	8.182	1.53	0.654	3.142
48	3.073	- 5.062	2.917	0.343	3.142
			2.834	0.397	

- **Sample no 20**

Table 5-4: showing sample no 20

ID	X	Y	Max	Min	Area
1	0	0	2.382	0.42	3.142
2	-1.026	1.361	4.144	0.241	3.142
3	2.063	0.438	2.651	0.377	3.142
4	0.745	-1.422	1.898	0.527	3.142

5	-2.551	-0.167	2.599	0.385	3.142
6	0.279	-2.37	2.916	0.343	3.142
7	4.951	1.86	2.852	0.351	3.142
8	3.072	-0.523	4.735	0.211	3.142
9	-3.358	1.383	2.053	0.487	3.142
10	8.227	2.328	2.108	0.474	3.142
11	2.254	-2.222	3.39	0.295	3.142
12	3.242	-2.862	1.856	0.539	3.142
13	-1.776	-1.602	1.765	0.567	3.142
14	-5.74	2.573	2.924	0.342	3.142
15	0.841	-3.791	4.288	0.233	3.142
16	4.667	0.583	1.589	0.629	3.142
17	0.204	-4.253	5.074	0.197	3.142
18	11.105	2.297	1.847	0.541	3.142
19	-7.502	3.899	1.66	0.602	3.142
20	5.206	-3.82	1.336	0.748	3.142
21	0.174	-4.983	1.912	0.523	3.142
22	-3.496	-5.642	9.179	0.109	3.142
23	-0.323	2.025	1.854	0.539	3.142
24	6.057	-2.938	2.43	0.411	3.142
25	-4.847	-1.477	4.698	0.213	3.142

26	0.975	3.068	1.602	0.624	3.142
27	-3.735	-6.185	2.335	0.428	3.142
28	7.645	-4.493	2.852	0.351	3.142
29	-9.341	4.449	6.801	0.147	3.142
30	-7.587	0.286	2.729	0.366	3.142
31	4.506	3.844	2.555	0.391	3.142
32	10.559	3.259	2.811	0.356	3.142
33	-7.662	5.383	1.718	0.582	3.142
34	7.734	4.886	2.084	0.48	3.142
35	-7.273	-1.525	2.289	0.437	3.142
36	-11.884	-3.179	3.22	0.311	3.142
38	-10.842	-1.064	3.474	0.288	3.142
39	11.64	4.608	4.187	0.239	3.142
40	-12.374	-1.215	5.23	0.191	3.142
41	-3.332	4.098	2.958	0.338	3.142
42	2.564	-5.202	5.416	0.185	3.142
43	-5.725	1.404	2.519	0.397	3.142
44	4.197	4.748	1.811	0.552	3.142
45	7.198	0.164	1.588	0.63	3.142
46	1.378	5.643	2.533	0.395	3.142
48	-4.701	-2.882	3.967	0.252	3.142

49	8.273	-1.539	4.782	0.209	3.142
50	4.675	-1.505	2.597	0.385	3.142
51	-2.332	-3.65	6.497	0.154	3.142
53	-0.094	-5.67	4.98	0.201	3.142
54	2.174	1.349	8.226	0.122	3.142
55	-6.485	-6.26	2.821	0.355	3.142
56	-4.471	-7.219	2.191	0.456	3.142
57	5.622	-6.891	3.31	0.302	3.142
58	5.807	- 5.461	2.765	0.362	3.142
			3.21796	0.378	

- **Sample no 22**

Table 5-5: showing sample no 22

ID	X	Y	Max	Min	Area
1	0	0	6.514	0.154	3.142
2	-0.031	0.531	2.765	0.362	3.142
3	0.475	-0.472	3.14	0.318	3.142
4	-1.417	-1.922	2.215	0.452	3.142
5	-2.793	-3.101	4.965	0.201	3.142
6	0.702	-2.019	2.086	0.479	3.142
7	0.171	1.596	1.488	0.672	3.142

8	0.55	2.883	2.182	0.458	3.142
9	3.009	-0.367	2.707	0.369	3.142
10	-2.376	1.197	2.668	0.375	3.142
11	-0.468	-4.232	2.308	0.433	3.142
12	-4.468	-2.152	3.844	0.26	3.142
13	3.865	1.512	2.288	0.437	3.142
14	-3.506	0.032	1.839	0.544	3.142
15	4.219	2.269	2.814	0.355	3.142
16	1.454	-5.31	3.065	0.326	3.142
17	4.18	2.915	5.961	0.168	3.142
18	6.15	1.854	7.913	0.126	3.142
19	-1.15	-5.115	1.79	0.559	3.142
20	3.517	4.108	2.242	0.446	3.142
21	3.167	-2.66	1.688	0.593	3.142
22	8.307	-1.571	2.8	0.357	3.142
23	-3.595	2.348	4.611	0.217	3.142
24	4.466	-3.74	3.483	0.287	3.142
25	11.702	-0.908	3.137	0.319	3.142
26	2.68	5	2.076	0.482	3.142
27	-0.992	4.639	2.231	0.448	3.142
28	4.658	5.557	4.098	0.244	3.142

29	-11.436	-6.587	9.841	0.102	3.142
30	-2.191	6.155	3.984	0.251	3.142
31	7.153	1.576	2.108	0.474	3.142
32	3.893	-5.412	2.182	0.458	3.142
33	0.796	7.548	1.846	0.542	3.142

- **Sample no 23**

Table 5-6: Showing sample no 23

ID	X	Y	Max	Min	Area
1	0	0	6.514	0.154	3.142
2	-0.031	0.531	2.765	0.362	3.142
3	0.475	-0.472	3.14	0.318	3.142
4	-1.417	-1.922	2.215	0.452	3.142
5	-2.793	-3.101	4.965	0.201	3.142
6	0.702	-2.019	2.086	0.479	3.142
7	0.171	1.596	1.488	0.672	3.142
8	0.55	2.883	2.182	0.458	3.142
9	3.009	-0.367	2.707	0.369	3.142
10	-2.376	1.197	2.668	0.375	3.142
11	-0.468	-4.232	2.308	0.433	3.142
12	-4.468	-2.152	3.844	0.26	3.142

13	3.865	1.512	2.288	0.437	3.142
14	-3.506	0.032	1.839	0.544	3.142
15	4.219	2.269	2.814	0.355	3.142
16	1.454	-5.31	3.065	0.326	3.142
17	4.18	2.915	5.961	0.168	3.142
18	6.15	1.854	7.913	0.126	3.142
19	-1.15	-5.115	1.79	0.559	3.142
20	3.517	4.108	2.242	0.446	3.142
21	3.167	-2.66	1.688	0.593	3.142
22	8.307	-1.571	2.8	0.357	3.142
23	-3.595	2.348	4.611	0.217	3.142
24	4.466	-3.74	3.483	0.287	3.142
25	11.702	-0.908	3.137	0.319	3.142
26	2.68	5	2.076	0.482	3.142
27	-0.992	4.639	2.231	0.448	3.142
28	4.658	5.557	4.098	0.244	3.142
29	-11.436	-6.587	9.841	0.102	3.142
30	-2.191	6.155	3.984	0.251	3.142
31	7.153	1.576	2.108	0.474	3.142
32	3.893	-5.412	2.182	0.458	3.142
33	0.796	7.548	1.846	0.542	3.142

34	1.711	8.773	2.013	0.497	3.142
35	-5.571	-2.139	8.94	0.112	3.142
36	-1.974	-5.994	2.17	0.461	3.142
37	4.692	-6.274	1.706	0.586	3.142
38	-0.727	-7.566	2.187	0.457	3.142
39	6.423	2.637	1.827	0.547	3.142
40	-3.819	2.918	2.571	0.389	3.142
41	-9.743	-3.151	4.776	0.209	3.142
42	-7.65	1.949	2.749	0.364	3.142
43	-4.377	3.68	4.997	0.2	3.142
44	-1.643	-8.882	3.688	0.271	3.142
45	-2.852	6.674	6.119	0.163	3.142
46	0.965	10.019	1.409	0.71	3.142
47	8.598	-7.538	3.342	0.299	3.142
48	-10.876	3.014	3.114	0.321	3.142
49	7.023	-3.186	2.122	0.471	3.142
50	3.958	10.17	5.478	0.183	3.142
51	5.852	10.517	2.463	0.406	3.142
52	-6.163	-0.564	2.642	0.378	3.142
53	-8.341	4.6	6.379	0.157	3.142
54	-1.324	8.428	2.642	0.379	3.142

55	9.984	4.712	3.21	0.312	3.142
56	2.652	-7.494	4.188	0.239	3.142
57	-7.353	-0.196	1.713	0.584	3.142
58	8.68	5.978	3.597	0.278	3.142
59	3.338	11.368	1.611	0.621	3.142
60	0.193	12.321	5.566	0.18	3.142
61	9.24	1.396	4.266	0.234	3.142
62	10.263	-2.364	1.577	0.634	3.142
64	-5.104	-6.728	2.688	0.372	3.142
65	-8.684	-4.589	1.395	0.717	3.142
66	6.609	0.317	3.208	0.312	3.142
68	3.726	12.272	5.117	0.195	3.142
69	9.589	5.181	4.052	0.247	3.142
			3.349	0.369	

References

Ahmad, A. R. (oct 2017). The Interrelationship of Micro-Meso and Macroscopic Structures on the western
limb of Hazara kashmir syntaxis Pakistan. *ACTA GEOLOGICA SINICA*, Vol. 91 No. 5 pp.1573–1623.

AKHTAR, Shamim, Yasin Rahim, Bin Hu, Hinyuen Tsang, Khawaja Ibrar, Muhammad Fahad Ullah, and al eh Ibrahim Bute. 019. " t ratigraphy and tr ucture of Dhamtaur Area, District Abbottabad, Eastern Hazara, Pakistan." *Open Journal of Geology* 09:57–66. doi: 10.4236/ojg.2019.91005.

Ali, A., Habib, U., Rehman, A. U., Zada, N., and Ismail, M., 2016. Tectonic Imprints of the Hazara Kashmir Syntaxis on the Mesozoic Rocks Exposed in Munda, Mohmand Agency, Northwest Pakistan. *Acta Geologica Sinica* (English Edition), 90(2): 440-455

Ali, Asghar, Sajjad Ahmad, Mohammad AsifKhan, Muhammad Khan, and Gohar Rehman. 2021. "Tectonic Framework of Northern Pakistan from Himalaya to Karakoram." Pp. 6 –412 in.

Ali, Asghar, Shah Faisal, Khaista Rehman, Suleman Khan, and Nijat Ullah. 0 15. "Tectonic Imprints of the Hazara Kashmir y ntaxis on the Northwest Himalayan Fold and Thrust Belt, North Pakistan." *Arabian Journal of Geosciences* 8. doi: 10.1007/s12517-015-1874-8.

Ali M. adeg h, Warren C. Young. n.d. "Roark's Formulas for t ress and train." *New York Chicago San Francisco Lisbon London Madrid Mexico City Milan New Delhi San Juan Seoul Singapore Sydney Toronto* Eighth Edition.

Anjum, M. N. (2022). A study of reservoir potential of Cretaceous–Paleocene successions of Nizampur basin, Khyber Pakhtunkhwa, Pakistan:. *constraints from fracture analysis, petrography and geochemistry. Carbonates and Evaporites*, 37(4), 1-19.

Anjum, Muhammad Naveed, Abbas Ali Naseem, Muhammad Yaseen, Ali Hasnain, Junaid Khan, and Jawad Ahmad. 0 . "A Study of Reservoir Potential of Cretaceous–Paleocene Successions of Nizampur Basin, Khyber Pakhtunkhwa, Pakistan: Constraints from Fracture Analysis, Petrography and Geochemistry." *Carbonates and Evaporites* 37(4):59. doi: 10.1007/s13146-022-00805-1.

Anon. 0 1. ""Kinematic Analysis and t rain.""

Anon. 0 . "Britannica, T. Information Architects of Encyclopaedia Geology." *Encyclopedia Britannica.*

Anon. (March 8). ""Britannica, T. Editors of Encyclopaedia.""

Anon. n.d.-a. "THE ARCHITECTURE OF EARTH' CONTINENTAL CRU T ." in *GEOLOGY 319 STRUCTURAL GEOLOG*.

Anon. n.d.-b. *The Journal of Strain Analysis for Engineering Design*. Committee on Publication Ethics (COPE).

Aslop, G.I., 1992. Progressive deformation and the rotation of contemporary fold axes in the Ballybofey Nappe, northwest Ireland. *Geological Journal,* 21: 271-285

Baig, Moazzam, Qamar Uz Zaman Dar, Fahad Zareef, Rana Ali, and Muhammad Jameel. 2022. " t ructural Interpretation and Time-Depth Conversion Based on 2D Seismic Data of Indus Offshore Area, Pakistan." 5 :1–12.

Bannister, R.A., 2004. *Normalized fry strain analysis of the Binnewater sandstone, central Hudson valley, New York* (Bachelor Thesis, College of Liberal Arts and Sciences University of Illinois Urbana-Champaign).

Bell, T.H., and Sanislav, I.V., 2011. A deformation partitioning approach to resolving the sequence of fold events and the orientations in which they formed across multiply deformed large-scale regions. *Journal of Structural Geology,* 33:1206- 1217.

Bell, T.H., Rieuwers, M.T., Cihan, M., Evans, T.P., Ham, A.P., and Welch P., 2013. Interrelationships between deformation partitioning, metamorphism and tectonism. *Tectonophysics,* 587:119-132.

Bossart, Paul, Dorothee Dietrich, Antonio Greco, Robert Ottiger, and John Ramsay. 1988. "The Tectonic Structure of the Hazara-Kashmir y ntaxis, out hern Himalayas, Pakistan." *Tectonics* 7:273–97. doi: 10.1029/TC007i002p00273.

Britannica, T. E. (2015). *Kābul River.* Encyclopedia Britannica https://www.britannica.com/place/Kabul River.

Calkins, James Alfred. 1967. *The Geology of the Western Limb of the Hazara-Kashmir Syntaxis, West Pakistan and Kashmir*. *Report*. 67–34. Reston, VA. doi: 10.3133/ofr6734.

Chew*, D. (29 (2003)). An Excel spreadsheet for finite strain analysis. Computers & Geosciences, 795 799.

contributors., W. ((2023).). Geography of Pakistan. In Wikipedia, The Free Encyclopedia.

contributors, Wikipedia. 0 . " t ress– t rain Analysis." *Stress-Strain Analysis*.

Danielle, Collins. 01 9. "Mechanical Properties of Materials: tress and t rain." *Linear Motion Tips*.

De Paor, Declan. 1980. " o me Limitations of the Rf/Phi Technique of t rain Analysis." *Tectonophysics* 64. doi: 10.1016/0040-1951(80)90257-7.

Drona Adhikari, C. B. (2021). REVIEW OF THE GEOLOGY OF THE ARUN-TAMOR REGION, EASTERN NEPAL:.

Fatmi, A. N.,. 19 1. "L ate Jurassic and Early Cretaceous Ammonites from hai kh Budin Hills, D. I. Khan (N. W. F. P.)." *Records of the Geological Survey of Pakistan* 2 1 (2),:22 .p., 7 pls.

Ghazi, Shahid, Syed Haroon Ali, Mohammad Sahraeyan, and Tanzila Hanif. 0 15. "An Overview of Tectonosedimentary Framework of the Salt Range, Northwestern Himalayan Fold and Thrust Belt, Pakistan." *Arabian Journal of Geosciences* 8(3):1635–51. doi: 10.1007/s12517-014-1284-3.

Hameed, Fahad, Muhammad Rustam Khan, and Michael Dentith. 0 . "C rustal tudy Based on Integrated Geophysical Techniques in the Northwestern Himalayas, Pakistan." *Geological Journal* 58(4):1523–49. doi: 10.1002/gj.4672.

Hussain, Hafiz, Maryam Fayaz, Muhammad Haneef, Dr Muhammad Hanif, Irfan Jan, and Bilal G. 2013. "Microfacies and Diagenetic-Fabric of the amana uk Formation at Harnoi ec tion." 46: 9 –91.

JPB. 019. "Du ctile Deformation-Concept of Finite train."

Journal of Institute of Science and Technology, , 26(2), 79-97 .
(n.d.). *Ductile deformation-Concepts of finite strain.*

Khan, Ahmad and , Osman al ad Hersi and a jjad Ahmed. 01 . " Lithologic and Biostratigraphic Properties of the Paleocene Lockhart Formation, Hazara and Potwar Basins, Northeast Pakistan: Preliminary Results."

Khan, Majid, and Yike Liu. 019. "Geo dynamic Evolution of the Offshore Indus Basin Pakistan: The Western Indian Plate Passive Continental Margin." *Geophysical Journal International*. doi: 10.1093/gji/ggz091.

Khan, Natasha, Khaista Rehman, Sajjad Ahmad, Jamil Khokher, Iqbal Hajana, and Dr Muhammad Hanif. 016. " e quence tratigraphic Analysis of Eocene Rock tr ata, Offshore Indus, out hwest Pakistan." *Marine Geophysical Research* 37. doi: 10.1007/s11001-016-9280-5.

Kumar, Pulkit, Moumita Mahanty, and Amares Chattopadhyay. 018. "An O rview of t ress-Strain Analysis for Elasticity Equations."

Kumar, Rajan, Deepak ri vastava, and Arun Kumar Ojha. 014. "A Comparison of the Methods for Objective t rain Estimation from the Fry Plots." *Journal of Structural Geology* 63. doi: 10.1016/j.jsg.2014.03.002.

Edward A. Johnson, P. D. (1999). *Lithofacies, Depositional Environments, and.* WASHINGTON UNITEDSTATES GOVERNMENT PRINTING OFFICE, .
(n.d.). *Folding/Faulting: Topographic Expression of Folded Strata.*

Hussain, M. F. ((2013)). Microfacies and diagenetic-fabric of the Samana Suk Formation at Harnoi Section.
Journal of Himalayan Earth Sciences, 79-91.

iqbal M.sheikh, m. k. (2007). environmental geology of islamabad rawalpindi northern pakistan. In P. D. Wardlaw, *regional studies of potwar plateau area northern pakistan* (p. chapter G). virginia: U.S geological
survey.

Jan, M. Q. (2020). Tectonic and structural analysis of the Balakot–Abbottabad section of Hazara-Kashmir syntaxis, northwestern Himalaya, Pakistan. *Journal of Himalayan Earth Sciences, 53(1), 1-16.*, 53(1), 1-16.

Kazmi, A. a. (1997). Geology and Tectonics of Pakistan. *Open Journal of Earthquake Research*, 554.
M. P. Searle, M. P. (2012). The Tectonic Evolution of the Karakoram and Western Himalaya. *Implications*

for the Development of the Tibetan Plateau, 353(1), 347-367.

M. Sadiq Malkani, Z. M. (2017). *STRATIGRAPHY OF PAKISTAN GSP Memoir Vol. 24.* Issued by Director
General, Geological Survey of Pakistan.

MALE UAV CFD Report, AvDI. (2018).
MonaLisa, A. A. ((Nov, 2005)). TECTONIC MODEL OF NW HIMALAYAN FOLD. *Pakistan Journal of Meteorology*.

Muhammad Qasim, M. A(2014). Stratigraphic characterization of the Early Cambrian Abbottabad Formation. *Journal of Himalayan Earth Sciences Volume 47, No. 1,*, 25-40.

Nelson, R. (. (n.d.). Geologic analysis of naturally fractured reservoirs. In *Elsevier.*

P. K. Zeitler, D. A. (1994). Tectonics of Nanga Parbat, Western Himalaya. *geology*, 999–1002.

Saboor, H. h. ((2020)). Sedimentological attributes of the Middle Jurassic peloids-dominated. *Carbonates
and Evaporites* , 35:123.

Shahid Hussain, M. F. (2018). Microfacies and and diagenetic fabrics of Samana Suk Formation at Harnoi.
journal of himlayan earth sciences, 51.Retrieved from https://link.springer.com/10.1007/s12583-021 1606-9

Waldron, J. W. (2016). https://courses.eas.ualberta.ca/. *kinematics*, p. part five.

Wardlaw, P. D. (2007). *Regional Studies of the potwar plateau area north pakistan.* USGS.

Qasim, Muhammad, Asif Khan, and Muhammad Haneef. 01 4. " tratigraphic Characterization of the Early Cambrian Abbottabad Formation in the Sherwan Area, Hazara Region, N. Pakistan: Implications for Early Paleozoic Stratigraphic Correlation in NW Himalayas, Pakistan." *Journal of Himalayan Earth Sciences* 47:25–40.

Raza, Auriba, Ift ikhar Raja, Elisabet Lindgren, and Shahid Raza. 2011. *Land-Use Change Analysis of District Abbottabad Using GIS and Remote Sensing*.

Samira, Taghdisi, Payman Rezaee, R. Moussavi-Harami, Mohammad Khanehbad, and Farzin Ghaemi. 019. "Fa cies Analysis, edimentary Environment and equen ce tratigraphy of the Khan Formation in the Kalmard Sub-Block, Central Iran: Implications for Lower Permian Palaeogeography." *Neues Jahrbuch Für Geologie Und Paläontologie - Abhandlungen* 292:129–54. doi: 10.1127/njgpa/2019/0812.

ear le, M., and Peter Treloar. 01 9. "An Introduction to Himalayan Tectonics: A Modern y nthesis." *Geological Society, London, Special Publications* 483:SP483-2019. doi: 10.1144/SP483-2019-20.

ear le, Michael P., Laurence J. Robb, and Nicholas J. Gardiner. 016. "Tectonic Processes and Metallogeny along the Tethyan Mountain Ranges of the Middle East and South Asia (Oman, Himalaya, Karakoram, Tibet, Myanmar, Thailand, Malaysia)." P. 0 in *Tectonics and Metallogeny of the Tethyan Orogenic Belt*. Vol. 19, edited by J. P. Richards. Society of Economic Geologists.

Shah, S. M. I. 1977. *Stratigraphy of Pakistan*. Director General, Geological Survey of Pakistan.

Shahzada, Khan, A. Naseer, and Mohammad Javed. 0 1 . " e ismic Hazard Assessment of Abbottabad City."

Tariq hak oor, Peter D. Warwick. n.d. "Lithofacies and Depositional Environments of the Coal-Bearing Paleocene Patala Formation, al t Range Coal Field, Northern Pakistan."

Wynne,A.B. 18 9. "A G eological Reconnaissance from the Indus at Kushalgarh to Kurram at Thal on Afghan Frontier." *Geological Survey India,* 12(2),:100-114.